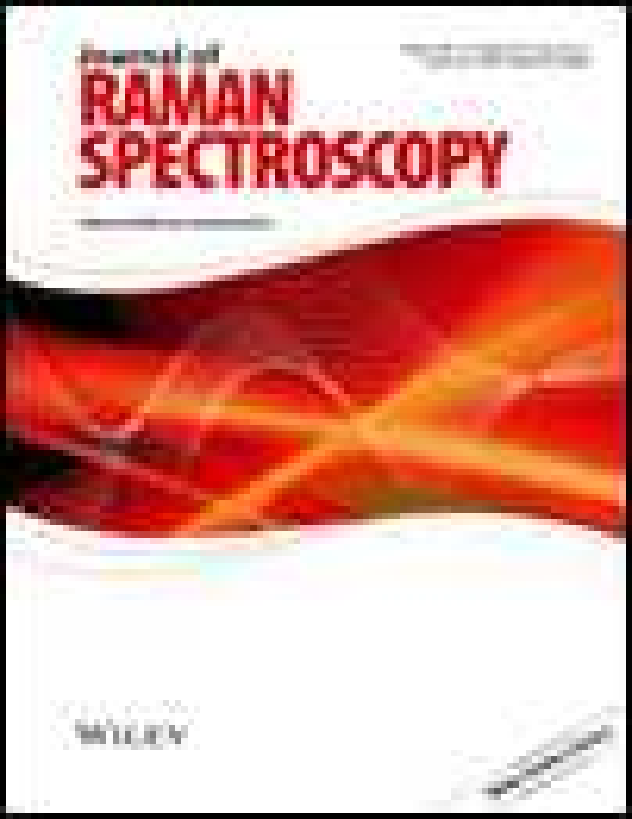
Journal of
RAMAN
SPECTROSCOPY
WILEY

Journal of Raman Spectroscopy

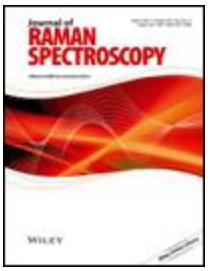

Impact Factor: 2.395

ISI Journal Citation Reports © Ranking: 2015: 15/43 (Spectroscopy)

Online ISSN: 1097-4555

Editorial Board

EDITOR-IN-CHIEF

Laurence A. Nafie
Department of Chemistry
Syracuse University
Syracuse, NY 13244-4100
USA.
lnafie@syr.edu (mailto:lnafie@syr.edu)

FOUNDING EDITOR EMERITUS

Derek A. Long
University of Bradford, UK

EDITOR EMERITUS

Wolfgang Kiefer
University of Wuerzburg, Germany

SENIOR ASSOCIATE EDITORS

Hiro-o Hamaguchi
Department of Applied Chemistry
and Institute of Molecular Science
College of Science
National Chiao Tung University
Taiwan
hhama@nctu.edu.tw
(mailto:hhama@nctu.edu.tw)

Lawrence D. Ziegler
Department of Chemistry
Boston University
590 Commonwealth Avenue
Boston, MA 02215
USA
lziegler@bu.edu
(mailto:lziegler@chem.bu.edu)

ASSOCIATE EDITORS

Philippe Colomban
Sorbonne Universite, Universite Pierre et
Marie Curie (Paris 06)
c49, 4 Place Jussieu
75005 Paris
France
philippe.colomban@upmc.fr
(mailto:philippe.colomban@glvt-cnrs.fr)

Tony Parker
STFC Rutherford Appleton Laboratory
Harwell Science and Innovation Campus
Didcot, Oxfordshire, OX11 0QX
United Kingdom
tony.parker@stfc.ac.uk
(mailto:tony.parker@stfc.ac.uk)

Juergen Popp
Institute of Photonic Technology
Albert-Einstein-Straße 9
07745 Jena
Germany
juergen.popp@uni-jena.de
(mailto:juergen.popp@uni-jena.de)

Giuletta Smulevich
Department of Chemistry
University of Florence
Via della Lastruccia 3
50019 Sesto Fiorentino (FI)
Italy
giulietta.smulevich@unifi.it
(mailto:giulietta.smulevich@unifi.it)

Zhong-Qun Tian
State Key Laboratory of Physical Chemistry
of Solid Surfaces
Xiamen University
Fujian Province
361005 China
zqtian@xmu.edu.cn
(mailto:zqtian@xmu.edu.cn)

EDITORIAL ADVISORY BOARD

Ricardo Aroca
University of Windsor, Canada

Sanford A. Asher
University of Pittsburgh, USA

Journal of Raman Spectroscopy

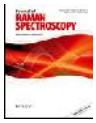

February 2017

Volume 48, Issue 2

Pages 143–347

1. **Issue information**

1. You have free access to this content
Issue information (pages 143–151) (/doi/10.1002/jrs.5018/full)

Version of Record online: 2 FEB 2017 | DOI: 10.1002/jrs.5018

- Abstract (/doi/10.1002/jrs.5018/abstract)
- Article (/doi/10.1002/jrs.5018/full)
- PDF(1362K) (/doi/10.1002/jrs.5018/epdf)
- PDF(1362K) (/doi/10.1002/jrs.5018/pdf)
- Request Permissions (https://s100.copyright.com/AppDispatchServlet?publisherName=Wiley&publication=JRS&title=Issue%20information&publicationDate=02%20FEB%202017&startPage=143&endPage=151&copyright=Copyright%20%C2%A9%202017%20John%20Wiley%20%2526%20Sons%2C%20Ltd.&contentID=10.1002%2Fjrs.5018&orderSource=onlinelibrary%7Cwol1%7Ctoc&orderBeanReset=true)

2. **Research articles**

1. Determination of skin penetration profiles by confocal Raman microspectroscopy: statistical evaluation of optimal microscope configuration (pages 152–160) (/doi/10.1002/jrs.5001/full)

Dominique Jasmin Lunter

Version of Record online: 11 AUG 2016 | DOI: 10.1002/jrs.5001

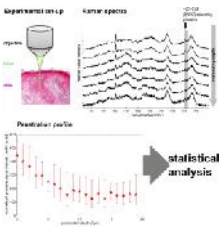

The aim of the study was to statistically evaluate the optimal microscope configuration for confocal Raman microspectroscopic determination of the penetration of a pharmaceutical active into the skin (depth profiling). A thorough statistical analysis using modified Bland–Altman plots and equivalence test of AUC values of penetration plots was carried out. It was found that both metallurgic and immersion objective can be used for depth profiling.

- Abstract (/doi/10.1002/jrs.5001/abstract)
- Article (/doi/10.1002/jrs.5001/full)
- PDF(389K) (/doi/10.1002/jrs.5001/epdf)
- PDF(389K) (/doi/10.1002/jrs.5001/pdf)
- References (/doi/10.1002/jrs.5001/full?scrollTo=references)
- Request Permissions (https://s100.copyright.com/AppDispatchServlet?publisherName=Wiley&publication=JRS&title=Determination%20of%20skin%20penetration%20profiles%20by%20confocal%20Raman%20microspectroscopy%3A%20statistical%20evaluation%20of%20optimal%20microscope%20configuration&publicationDate=11%20AUG%202016&author=Dominique%20Jasmin%20Lunter&startPage=152&endPage=160&copyright=Copyright%20%C2%A9%202016%20John%20Wiley%20%2526%20Sons%2C%20Ltd.&contentID=10.1002%2Fjrs.5001&orderSource=onlinelibrary%7Cwol1%7Ctoc&orderBeanReset=true)

2. Biomineralization in saxicolous lichens: Raman spectroscopic study supported with XRF and SEM-EDX analyses (pages 161–169) (/doi/10.1002/jrs.5015/full)

I. Ibarrondo, I. Martínez-Arkarazo and J. M. Madariaga

Version of Record online: 24 AUG 2016 | DOI: 10.1002/jrs.5015

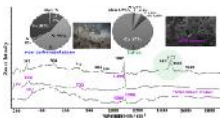

The biominerals accumulated on several stone materials colonized by saxicolous lichens living under different environmental conditions are characterized. The work describes the calcium oxalate distribution on the surface of caloplaca and lecanoraceae lichen genera and demonstrates the neogenesis of calcium oxalates on non carbonated stones (where X-ray spectroscopy evidenced the absence of calcium) suggesting an atmospheric uptake.

It is noticeable the detection of calcite ($CaCO_3$), ankerite ($FeCa(CO_3)_2$) and dolomite ($CaMg(CO_3)_2$) in the vicinity of the lichen thalli. These evidences are described by means of Raman spectroscopy for the first time.

- Abstract (/doi/10.1002/jrs.5015/abstract)
- Article (/doi/10.1002/jrs.5015/full)
- PDF(535K) (/doi/10.1002/jrs.5015/epdf)
- PDF(535K) (/doi/10.1002/jrs.5015/pdf)
- References (/doi/10.1002/jrs.5015/full?scrollTo=references)
- Request Permissions (https://s100.copyright.com/AppDispatchServlet?publisherName=Wiley&publication=JRS&title=Biomineralization%20in%20saxicolous%20lichens%3A%20Raman%20spectroscopic%20study%20supported%20with%20XRF%20and%20SEM-EDX%20analyses&publicationDate=24%20AUG%202016&author=I.%20Ibarrondo%2CI.%20Mart%C3%ADnez-Arkarazo%2CJ.%20M.%20Madariaga&startPage=161&endPage=169&copyright=Copyright%20%C2%A9%202016%20John%20Wiley%20%2526%20Sons%2C%20Ltd.&contentID=10.1002%2Fjrs.5015&orderSource=onlinelibrary%7Cwol1%7Ctoc&orderBeanReset=true)

3. Structural characterization of phosphatidylglycerol model membranes containing the antibiotic target lipid II molecule: a Raman microspectroscopy study (pages 170–179) (/doi/10.1002/jrs.5033/full)

M. C. Sosa Morales and R. M. S. Álvarez

Version of Record online: 21 SEP 2016 | DOI: 10.1002/jrs.5033

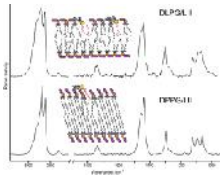

Antibiotics realize their function via interaction with lipid II (LII), a component of the bacterial membrane. We evaluate by Raman microspectroscopy the modifications induced by LII in model anionic membranes in two different lipid states in order to reach a profound characterization of these systems that mimic the bacterial membrane and supply a solid platform to further studies regarding the recognition process of LII receptor by antibiotics.

- Abstract (/doi/10.1002/jrs.5033/abstract)
- Article (/doi/10.1002/jrs.5033/full)
- PDF(638K) (/doi/10.1002/jrs.5033/epdf)
- PDF(638K) (/doi/10.1002/jrs.5033/pdf)
- References (/doi/10.1002/jrs.5033/full?scrollTo=references)
- Request Permissions (https://s100.copyright.com/AppDispatchServlet?publisherName=Wiley&publication=JRS&title=Structural%20characterization%20of%20phosphatidylglycerol%20model%20membranes%20containing%20the%20antibiotic%20target%20lipid%20II%20molecule%3A%20a%20Raman%20microspectroscopy%20study&publicationDate=21%20SEP%202016&author=M.%20C.%20Sosa%20Morales%2CR.%20M.%20S.%20%C3%81lvarez&startPage=170&endPage=179&copyright=Copyright%20%C2%A9%202016%20John%20Wiley%20%2526%20Sons%2C%20Ltd.&contentID=10.1002%2Fjrs.5033&orderSource=onlinelibrary%7Cwol1%7Ctoc&orderBeanReset=true)

4. Application of resonance Raman spectroscopy for interrogation of cryoradiolytically reduced oxygenated heme proteins (pages 180–190) (/doi/10.1002/jrs.5038/full)

   Ying Wang, Piotr J. Mak, Qianhong Zhu and James R. Kincaid

   Version of Record online: 21 SEP 2016 | DOI: 10.1002/jrs.5038

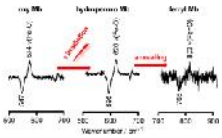

Resonance Raman (rR) spectroscopy can effectively interrogate unstable intermediates that arise in the enzymatic cycles of heme enzymes, such as peroxo-, hydroperoxo- and ferryl species. Though typically difficult to trap these elusive intermediates in solution, the cryoradiolysis approach offers a way to successfully do so. The present work employs modified derivatives of myoglobin to demonstrate the utility of this combination of rR and cryoradiolysis for structural characterization of these reactive Fe—O—O, Fe—O—O—H and Fe═O fragments of such reactive species.

- Abstract (/doi/10.1002/jrs.5038/abstract)
- Article (/doi/10.1002/jrs.5038/full)
- PDF(1012K) (/doi/10.1002/jrs.5038/epdf)
- PDF(1012K) (/doi/10.1002/jrs.5038/pdf)
- References (/doi/10.1002/jrs.5038/full?scrollTo=references)
- Request Permissions (https://s100.copyright.com/AppDispatchServlet?publisherName=Wiley&publication=JRS&title=Application%20of%20resonance%20Raman%20spectroscopy%20for%20interrogation%20of%20cryoradiolytically%20reduced%20oxygenated%20heme%20proteins&publicationDate=21%20SEP%202016&author=Ying%20Wang%2CPiotr%20J.%20Mak%2CQianhong%20Zhu%2CJames%20R.%20Kincaid&startPage=180&endPage=190&copyright=Copyright%20%C2%A9%202016%20John%20Wiley%20%2526%20Sons%2C%20Ltd.&contentID=10.1002%2Fjrs.5038&orderSource=onlinelibrary%7Cwol1%7Ctoc&orderBeanReset=true)

5. Tip-enhanced Raman mapping of single-walled carbon nanotube networks in conductive composite materials (pages 191–196) (/doi/10.1002/jrs.5004/full)

   Günter G. Hoffmann, Oana A. Bârsan, Leendert G. J. van der Ven and Gijsbertus de With

   Version of Record online: 29 JUL 2016 | DOI: 10.1002/jrs.5004

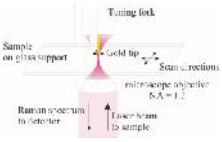

Using tip-enhanced Raman spectroscopy, the surface of a polymer-embedded conductive network of SWCNTs was mapped underneath a thin layer of pure polymer for the first time. The technique was also used to detect tube-breaking within the composite sample caused by mechanical stress.

- Abstract (/doi/10.1002/jrs.5004/abstract)
- Article (/doi/10.1002/jrs.5004/full)
- PDF(495K) (/doi/10.1002/jrs.5004/epdf)
- PDF(495K) (/doi/10.1002/jrs.5004/pdf)
- References (/doi/10.1002/jrs.5004/full?scrollTo=references)
- Request Permissions (https://s100.copyright.com/AppDispatchServlet?publisherName=Wiley&publication=JRS&title=Tip-enhanced%20Raman%20mapping%20of%20single-walled%20carbon%20nanotube%20networks%20in%20conductive%20composite%20materials&publicationDate=29%20JUL%202016&author=G%C3%BCnter%20G.%20Hoffmann%2COana%20A.%20B%C3%A2rsan%2CLeendert%20G.%20J.%20Ven%2CGijsbertus%20With&startPage=191&endPage=196&copyright=Copyright%20%C2%A9%202016%20John%20Wiley%20%2526%20Sons%2C%20Ltd.&contentID=10.1002%2Fjrs.5004&orderSource=onlinelibrary%7Cwol1%7Ctoc&orderBeanReset=true)

6. Shell-isolated nanoparticle-enhanced Raman spectroscopy characterization of oxide ores during thiosulfate-mediated gold leaching (pages 197–203) (/doi/10.1002/jrs.5011/full)

   Scott R. Smith, Janet Y. Baron, Yeonuk Choi and Jacek Lipkowski

   Version of Record online: 11 AUG 2016 | DOI: 10.1002/jrs.5011

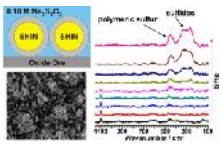

Shell-isolated nanoparticle-enhanced Raman spectroscopy was employed to study oxide ores exposed to a thiosulfate solution. The passive layer was found to consist of metal sulfides and polysulfide chains. A pressure oxidation pretreatment process minimized the mineral catalysed thiosulfate decomposition.

- Abstract (/doi/10.1002/jrs.5011/abstract)
- Article (/doi/10.1002/jrs.5011/full)
- PDF(401K) (/doi/10.1002/jrs.5011/epdf)
- PDF(401K) (/doi/10.1002/jrs.5011/pdf)
- References (/doi/10.1002/jrs.5011/full?scrollTo=references)
- Request Permissions (https://s100.copyright.com/AppDispatchServlet?publisherName=Wiley&publication=JRS&title=Shell-isolated%20nanoparticle-enhanced%20Raman%20spectroscopy%20characterization%20of%20oxide%20ores%20during%20thiosulfate-mediated%20gold%20leaching&publicationDate=11%20AUG%202016&author=Scott%20R.%20Smith%2CJanet%20Y.%20Baron%2CYeonuk%20Choi%2CJacek%20Lipkowski&startPage=197&endPage=203&copyright=Copyright%20%C2%A9%202016%20John%20Wiley%20%2526%20Sons%2C%20Ltd.&contentID=10.1002%2Fjrs.5011&orderSource=onlinelibrary%7Cwol1%7Ctoc&orderBeanReset=true)

7. Selective detection of chloramphenicol in milk based on a molecularly imprinted polymer–surface-enhanced Raman spectroscopic nanosensor (pages 204–210) (/doi/10.1002/jrs.5034/full)

   Yunfei Xie, Mengyao Zhao, Qi Hu, Yuliang Cheng, Yahui Guo, He Qian and Weirong Yao

   Version of Record online: 29 SEP 2016 | DOI: 10.1002/jrs.5034

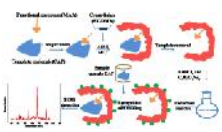

In agriculture pesticides are delivered as sprays which consist of microdroplets. Many pesticides contain aromatic compounds to which very often Cl-atoms and, more rarely, NO_2-groups are attached. We have chosen 3-Chlorophenol (1) and 4-Chloro-2-nitrobenzoic acid (2) as model substances according to their good solubility in water as the most common solvent in nature. For the remote detection of those components in single water droplets, external seeding of stimulated Raman scattering has been used.

- Abstract (/doi/10.1002/jrs.5034/abstract)
- Article (/doi/10.1002/jrs.5034/full)
- PDF(929K) (/doi/10.1002/jrs.5034/epdf)
- PDF(929K) (/doi/10.1002/jrs.5034/pdf)
- References (/doi/10.1002/jrs.5034/full?scrollTo=references)
- Request Permissions (https://s100.copyright.com/AppDispatchServlet?publisherName=Wiley&publication=JRS&title=Selective%20detection%20of%20chloramphenicol%20in%20milk%20based%20on%20a%20molecularly%20imprinted%20polymer%E2%80%93surface-enhanced%20Raman%20spectroscopic%20nanosensor&publicationDate=29%20SEP%202016&author=Yunfei%20Xie%2CMengyao%20Zhao%2CQi%20Hu%2CYuliang%20Cheng%2CYahui%20Guo%2CHe%20Qian%2CWeirong%20Yao&startPage=204&endPage=210&copyright=Copyright%20%C2%A9%202016%20John%20Wiley%20%2526%20Sons%2C%20Ltd.&contentID=10.1002%2Fjrs.5034&orderSource=onlinelibrary%7Cwol1%7Ctoc&orderBeanReset=true)

8. SERS optical fiber probe with plasmonic end-facet (pages 211–216) (/doi/10.1002/jrs.5031/full)

   Ming Xia, Pei Zhang, Claris Leung and Ya-Hong Xie

   Version of Record online: 14 SEP 2016 | DOI: 10.1002/jrs.5031

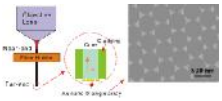

   This work presents the experimental and theoretical studies of an optical fiber probe with nano-structured end-facet for bio-sensing applications via surface-enhanced Raman spectroscopy. The factors affecting the intensity of Raman signal passing through the fiber probe are investigated. A hybrid graphene/Au nano-triangle structure is also transferred on the end-facet of the fiber probe to enable surface-enhanced Raman spectroscopy.

   - Abstract (/doi/10.1002/jrs.5031/abstract)
   - Article (/doi/10.1002/jrs.5031/full)
   - PDF(703K) (/doi/10.1002/jrs.5031/epdf)
   - PDF(703K) (/doi/10.1002/jrs.5031/pdf)
   - References (/doi/10.1002/jrs.5031/full?scrollTo=references)
   - Request Permissions (https://s100.copyright.com/AppDispatchServlet?publisherName=Wiley&publication=JRS&title=SERS%20optical%20fiber%20probe%20with%20plasmonic%20end-facet&publicationDate=14%20SEP%202016&author=Ming%20Xia%2CPei%20Zhang%2CClaris%20Leung%2CYa-Hong%20Xie&startPage=211&endPage=216&copyright=Copyright%20%C2%A9%202016%20John%20Wiley%20%2526%20Sons%2C%20Ltd.&contentID=10.1002%2Fjrs.5031&orderSource=onlinelibrary%7Cwol1%7Ctoc&orderBeanReset=true)

9. Surface-enhanced Raman scattering from plasmonic Ag-nanocube@Au-nanospheres core@satellites (pages 217–223) (/doi/10.1002/jrs.5032/full)

   Zhulin Huang, Guowen Meng, Qing Huang, Bin Chen, Yilin Lu, Zhaoming Wang, Xiaoguang Zhu and Kexi Sun

   Version of Record online: 14 SEP 2016 | DOI: 10.1002/jrs.5032

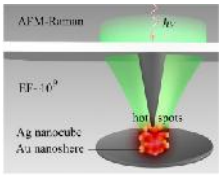

   Owning to the hot spots from sharp edged Ag-nanocube and nanoscaled gaps between the Au-nanosphere satellites and Ag-nanocube cores, the Raman enhancement factor of singular Ag-nanocube@Au-nanospheres core@satellites analogue can be up to 3.4×10^8, while that of a Ag-nanocube is 1.5×10^8.

   - Abstract (/doi/10.1002/jrs.5032/abstract)
   - Article (/doi/10.1002/jrs.5032/full)
   - PDF(579K) (/doi/10.1002/jrs.5032/epdf)
   - PDF(579K) (/doi/10.1002/jrs.5032/pdf)
   - References (/doi/10.1002/jrs.5032/full?scrollTo=references)
   - Request Permissions (https://s100.copyright.com/AppDispatchServlet?publisherName=Wiley&publication=JRS&title=Surface-enhanced%20Raman%20scattering%20from%20plasmonic%20Ag-nanocube%40Au-nanospheres%20core%40satellites&publicationDate=14%20SEP%202016&author=Zhulin%20Huang%2CGuowen%20Meng%2CQing%20Huang%2CBin%20Chen%2CYilin%20Lu%2CZhaoming%20Wang%2CXiaoguang%20Zhu%2CKexi%20Sun&startPage=217&endPage=223&copyright=Copyright%20%C2%A9%202016%20John%20Wiley%20%2526%20Sons%2C%20Ltd.&contentID=10.1002%2Fjrs.5032&orderSource=onlinelibrary%7Cwol1%7Ctoc&orderBeanReset=true)

10. Resonant Raman scattering in nanocrystalline thin CdS film (pages 224–229) (/doi/10.1002/jrs.5002/full)

    Muhammad Farooq Saleem, Hua Zhang, Yi Deng and Deliang Wang

    Version of Record online: 29 JUL 2016 | DOI: 10.1002/jrs.5002

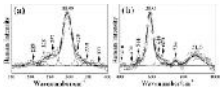

    Surface-enhanced Raman scattering and resonant Raman scattering are concurrently achieved by employing silver nanoparticles and by adjusting the band gap of cadmium sulfide through annealing. The much enhanced Raman scattering made it possible to *in situ* monitor annealing-induced phase transition and to observe multi-phonon modes and their replicas that are hardly detectable in a normal Raman scattering setup.

    - Abstract (/doi/10.1002/jrs.5002/abstract)
    - Article (/doi/10.1002/jrs.5002/full)
    - PDF(528K) (/doi/10.1002/jrs.5002/epdf)
    - PDF(528K) (/doi/10.1002/jrs.5002/pdf)
    - References (/doi/10.1002/jrs.5002/full?scrollTo=references)
    - Request Permissions (https://s100.copyright.com/AppDispatchServlet?publisherName=Wiley&publication=JRS&title=Resonant%20Raman%20scattering%20in%20nanocrystalline%20thin%20CdS%20film&publicationDate=29%20JUL%202016&author=Muhammad%20Farooq%20Saleem%2CHua%20Zhang%2CYi%20Deng%2CDeliang%20Wang&startPage=224&endPage=229&copyright=Copyright%20%C2%A9%202016%20John%20Wiley%20%2526%20Sons%2C%20Ltd.&contentID=10.1002%2Fjrs.5002&orderSource=onlinelibrary%7Cwol1%7Ctoc&orderBeanReset=true)

11. You have free access to this content
    Resonance Raman of oxygen dangling bonds in amorphous silicon dioxide (pages 230–234) (/doi/10.1002/jrs.5006/full)

    D. Di Francesca, A. Boukenter, S. Agnello, A. Alessi, S. Girard, M. Cannas and Y. Ouerdane

    Version of Record online: 3 AUG 2016 | DOI: 10.1002/jrs.5006

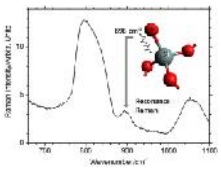

    We studied a resonance Raman band peaking at 896 cm^{-1}, which can be easily revealed in silica glass rich of oxygen-excess related point defects. On the basis of experimental evidences, the band is assigned to non-bridging oxygen hole centers.

    - Abstract (/doi/10.1002/jrs.5006/abstract)
    - Article (/doi/10.1002/jrs.5006/full)
    - PDF(354K) (/doi/10.1002/jrs.5006/epdf)
    - PDF(354K) (/doi/10.1002/jrs.5006/pdf)
    - References (/doi/10.1002/jrs.5006/full?scrollTo=references)
    - Request Permissions (https://s100.copyright.com/AppDispatchServlet?publisherName=Wiley&publication=JRS&title=Resonance%20Raman%20of%20oxygen%20dangling%20bonds%20in%20amorphous%20silicon%20dioxide&publicationDate=03%20AUG%202016&author=D.%20Di%20Francesca%2CA.%20Boukenter%2CS.%20Agnello%2CA.%20Alessi%2CS.%20Girard%2CM.%20Cannas%2CY.%20Ouerdane&startPage=230&endPage=234&copyright=Copyright%20%C2%A9%202016%20John%20Wiley%20%2526%20Sons%2C%20Ltd.&contentID=10.1002%2Fjrs.5006&orderSource=onlinelibrary%7Cwol1%7Ctoc&orderBeanReset=true)

12. Surface-directed molecular assembly of pentacene on aromatic organophosphonate self-assembled monolayers explored by polarized Raman spectroscopy (pages 235–242) (/doi/10.1002/jrs.5007/full)

    Sara Yazji, Christian Westermeier, Dominik Weinbrenner, Matthias Sachsenhauser, Kung-Ching Liao, Simon Noever, Paolo Postorino, Jeffrey Schwartz, Gerhard Abstreiter, Bert Nickel, Ilaria Zardo and Anna Cattani-Scholz

    Version of Record online: 15 AUG 2016 | DOI: 10.1002/jrs.5007

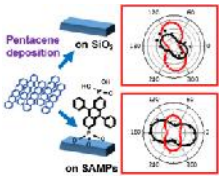

Raman spectroscopy is used to probe the degree of anisotropy in pentacene thin films deposited on three structurally different aromatic organophosphonate self-assembled monolayers.

- Abstract (/doi/10.1002/jrs.5007/abstract)
- Article (/doi/10.1002/jrs.5007/full)
- PDF(561K) (/doi/10.1002/jrs.5007/epdf)
- PDF(561K) (/doi/10.1002/jrs.5007/pdf)
- References (/doi/10.1002/jrs.5007/full?scrollTo=references)
- Request Permissions (https://s100.copyright.com/AppDispatchServlet?publisherName=Wiley&publication=JRS&title=Surface-directed%20molecular%20assembly%20of%20pentacene%20on%20aromatic%20organophosphonate%20self-assembled%20monolayers%20explored%20by%20polarized%20Raman%20spectroscopy&publicationDate=15%20AUG%202016&author=Sara%20Yazji%2CChristian%20Westermeier%2CDominik%20Weinbrenner%2CMatthias%20Sachsenhauser%2CKung-Ching%20Liao%2CSimon%20Noever%2CPaolo%20Postorino%2CJeffrey%20Schwartz%2CGerhard%20Abstreiter%2CBert%20Nickel%2CIlaria%20Zardo%2CAnna%20Cattani-Scholz&startPage=235&endPage=242&copyright=Copyright%20%C2%A9%202016%20John%20Wiley%20%2526%20Sons%2C%20Ltd.&contentID=10.1002%2Fjrs.5007&orderSource=onlinelibrary%7Cwol1%7Ctoc&orderBeanReset=true)

13. Laser-induced plasmonic heating on silver nanoparticles/poly(*N*-isopropylacrylamide) mats for optimizing SERS detection (pages 243–250) (/doi/10.1002/jrs.5012/full)

    Lin Wang, Yan Zhang, Wenqi Zhang, Tianrui Ren, Feng Wang and Haifeng Yang

    Version of Record online: 8 AUG 2016 | DOI: 10.1002/jrs.5012

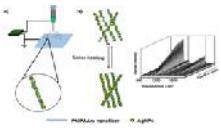

Silver nanoparticle/poly(*N*-isopropylacrylamide) composite nanofibers fabricated by electrospinning have enhanced surface-enhanced Raman scattering (SERS) effect upon continuous pulsed laser irradiation, showing a 'laser heating sensitive' SERS effect. Laser-induced plasmonic heating can also tune the temperature-responsive interaction between poly(*N*-isopropylacrylamide) and analytes and have been utilized in the on-site 'laser heating sensitive' separation and SERS detection of analytes.

- Abstract (/doi/10.1002/jrs.5012/abstract)
- Article (/doi/10.1002/jrs.5012/full)
- PDF(807K) (/doi/10.1002/jrs.5012/epdf)
- PDF(807K) (/doi/10.1002/jrs.5012/pdf)
- References (/doi/10.1002/jrs.5012/full?scrollTo=references)
- Request Permissions (https://s100.copyright.com/AppDispatchServlet?publisherName=Wiley&publication=JRS&title=Laser-induced%20plasmonic%20heating%20on%20silver%20nanoparticles%2Fpoly%28N-isopropylacrylamide%29%20mats%20for%20optimizing%20SERS%20detection&publicationDate=08%20AUG%202016&author=Lin%20Wang%2CYan%20Zhang%2CWenqi%20Zhang%2CTianrui%20Ren%2CFeng%20Wang%2CHaifeng%20Yang&startPage=243&endPage=250&copyright=Copyright%20%C2%A9%202016%20John%20Wiley%20%2526%20Sons%2C%20Ltd.&contentID=10.1002%2Fjrs.5012&orderSource=onlinelibrary%7Cwol1%7Ctoc&orderBeanReset=true)

14. High resolution stimulated Raman spectroscopy from collisionally populated states after optical pumping: the $3\nu_2 \leftarrow 2\nu_2$ and $\nu_3+2\nu_4+\nu_5 \leftarrow 2\nu_4+\nu_5$ *Q* branches of $^{12}C_2H_2$ and the $3\nu_2 \leftarrow 2\nu_2$ *Q* branch of $^{12}C_2D_2$. (pages 251–257) (/doi/10.1002/jrs.5005/full)

    Raúl Z. Martínez, Dionisio Bermejo, Gianfranco Di Lonardo and Luciano Fusina

    Version of Record online: 17 AUG 2016 | DOI: 10.1002/jrs.5005

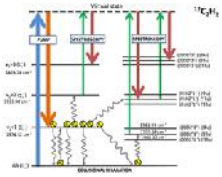

A combination of a pump-probe double resonance Raman technique and the naturally occurring process of vibration-to-vibration collisional relaxation is used to populate and obtain high resolution Raman spectra of vibrationally excited states, which are difficult to access by other means.

- Abstract (/doi/10.1002/jrs.5005/abstract)
- Article (/doi/10.1002/jrs.5005/full)
- PDF(290K) (/doi/10.1002/jrs.5005/epdf)
- PDF(290K) (/doi/10.1002/jrs.5005/pdf)
- References (/doi/10.1002/jrs.5005/full?scrollTo=references)
- Request Permissions (https://s100.copyright.com/AppDispatchServlet?publisherName=Wiley&publication=JRS&title=High%20resolution%20stimulated%20Raman%20spectroscopy%20from%20collisionally%20populated%20states%20after%20optical%20pumping%3A%20the%203%CE%BD2%E2%86%902%CE%BD2%20and%20%CE%BD2%2B%CE%BD4%2B%CE%BD5%E2%86%902%CE%BD4%2B%CE%BD5%E2%80%89Q%20branches%20of%2012C2H2%20and%20the%203%CE%BD2%E2%86%902%CE%BD2%E2%80%89Q%20branch%20of%2012C2D2.&publicationDate=17%20AUG%202016&author=Ra%C3%BAl%20Z.%20Mart%C3%ADnez%2CDionisio%20Bermejo%2CGianfranco%20Di%20Lonardo%2CLuciano%20Fusina&startPage=251&endPage=257&copyright=Copyright%20%C2%A9%202016%20John%20Wiley%20%2526%20Sons%2C%20Ltd.&contentID=10.1002%2Fjrs.5005&orderSource=onlinelibrary%7Cwol1%7Ctoc&orderBeanReset=true)

15. Characterization of archaeometallurgical artefacts by means of portable Raman systems: corrosion mechanisms influenced by marine aerosol (pages 258–266) (/doi/10.1002/jrs.4997/full)

    M. Veneranda, J. Aramendia, O. Gomez, S. Fdez-Ortiz de Vallejuelo, L. Garcia, I. Garcia-Camino, K. Castro, A. Azkarate and J. M. Madariaga

    Version of Record online: 8 AUG 2016 | DOI: 10.1002/jrs.4997

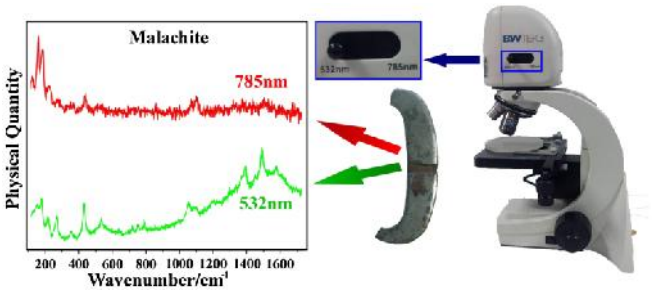

The main corrosion phases affecting several archaeometallurgical artefacts proceeding from the Ereñozar necropolis (13th century, Basque Country, Spain) were characterized through the use of portable Raman systems. Thanks to the dual laser wavelength port of the coupled BAC151B video microscope, it was possible to focus on the same spots of analysis with both 532 and 785 nm lasers. The obtained results emphasize that by using different excitation sources in a complementary way, it is possible to maximize the molecular information provided by Raman spectroscopy.

- Abstract (/doi/10.1002/jrs.4997/abstract)
- Article (/doi/10.1002/jrs.4997/full)
- PDF(507K) (/doi/10.1002/jrs.4997/epdf)
- PDF(507K) (/doi/10.1002/jrs.4997/pdf)
- References (/doi/10.1002/jrs.4997/full?scrollTo=references)
- Request Permissions (https://s100.copyright.com/AppDispatchServlet?publisherName=Wiley&publication=JRS&title=Characterization%20of%20archaeometallurgical%20artefacts%20by%20means%20of%20portable%20Raman%20systems%3A%20corrosion%20mechanisms%20influenced%20by%20marine%20aerosol&publicationDate=08%20AUG%202016&author=M.%20Veneranda%2CJ.%20Aramendia%2CO.%20Gomez%2CS.%20Fdez-Ortiz%20de%20Vallejuelo%2CL.%20Garcia%2CI.%20Garcia-Camino%2CK.%20Castro%2CA.%20Azkarate%2CJ.%20M.%20Madariaga&startPage=258&endPage=266&copyright=Copyright%20%C2%A9%202016%20John%20Wiley%20%2526%20Sons%2C%20Ltd.&contentID=10.1002%2Fjrs.4997&orderSource=onlinelibrary%7Cwol1%7Ctoc&orderBeanReset=true)

16. Raman study of Yuan Qinghua porcelain: the highlighting of dendritic $CoFe_2O_4$ crystals in blue decorations (pages 267–270) (/doi/10.1002/jrs.5029/full)

    Tian Wang, Tiequan Zhu, Magali Brunet, Christophe Deshayes and Philippe Sciau

    Version of Record online: 21 SEP 2016 | DOI: 10.1002/jrs.5029

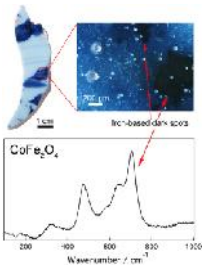

For Yuan productions, the blue decors present dark spots contrasting finely with the blue parts. It is currently believed that the dark spots are attributed to magnetite (Fe_3O_4). Nevertheless, in our work for the first time dendritic cobalt ferrite ($CoFe_2O_4$) crystals were observed by scanning electron microscopy and Raman spectroscopy as the main constituent of the dark spots. Through investigations, there were two types of populations existed in these spinel crystals—spinel richer in iron ($Co_{3-x}Fe_xO_4$, $x > 2$) and spinel richer in cobalt ($Co_{3-x}Fe_xO_4$, $x < 2$). Both cause the blackening of the blue decors.

- Abstract (/doi/10.1002/jrs.5029/abstract)
- Article (/doi/10.1002/jrs.5029/full)
- PDF(451K) (/doi/10.1002/jrs.5029/epdf)
- PDF(451K) (/doi/10.1002/jrs.5029/pdf)
- References (/doi/10.1002/jrs.5029/full?scrollTo=references)
- Request Permissions (https://s100.copyright.com/AppDispatchServlet?publisherName=Wiley&publication=JRS&title=Raman%20study%20of%20Yuan%20Qinghua%20porcelain%3A%20the%20highlighting%20of%20dendritic%20CoFe2O4%20crystals%20in%20blue%20decorations&publicationDate=21%20SEP%202016&author=Tian%20Wang%2CTiequan%20Zhu%2CMagali%20Brunet%2CChristophe%20Deshayes%2CPhilippe%20Sciau&startPage=267&endPage=270&copyright=Copyright%20%C2%A9%202016%20John%20Wiley%20%2526%20Sons%2C%20Ltd.&contentID=10.1002%2Fjrs.5029&orderSource=onlinelibrary%7Cwol1%7Ctoc&orderBeanReset=true)

17. Solid-state photodimerization of 9-methyl-anthracene (pages 271–277) (/doi/10.1002/jrs.5003/full)

Tommaso Salzillo, Elisabetta Venuti, Raffaele Guido Della Valle and Aldo Brillante

Version of Record online: 29 JUL 2016 | DOI: 10.1002/jrs.5003

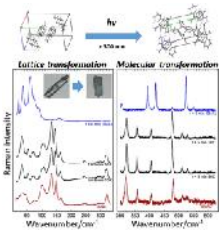

Raman microscopy has been used to study the crystal-to-crystal photodimerization of 9-methyl-anthracene, analyzing the time evolution of both the molecular and the lattice phonon spectra during the transformation from the reactant to the product. This has made possible the concomitant detection of the chemical and crystal lattice changes in the same portion of the irradiated crystal. The topochemical mechanism of this reaction produces a fast process leading to a complete transformation of the monomer into the dimer.

- Abstract (/doi/10.1002/jrs.5003/abstract)
- Article (/doi/10.1002/jrs.5003/full)
- PDF(526K) (/doi/10.1002/jrs.5003/epdf)
- PDF(526K) (/doi/10.1002/jrs.5003/pdf)
- References (/doi/10.1002/jrs.5003/full?scrollTo=references)
- Request Permissions (https://s100.copyright.com/AppDispatchServlet?publisherName=Wiley&publication=JRS&title=Solid-state%20photodimerization%20of%209-methyl-anthracene&publicationDate=29%20JUL%202016&author=Tommaso%20Salzillo%2CElisabetta%20Venuti%2CRaffaele%20Guido%20Della%20Valle%2CAldo%20Brillante&startPage=271&endPage=277&copyright=Copyright%20%C2%A9%202016%20John%20Wiley%20%2526%20Sons%2C%20Ltd.&contentID=10.1002%2Fjrs.5003&orderSource=onlinelibrary%7Cwol1%7Ctoc&orderBeanReset=true)

18. Single particle structure characterization of solid-state synthesized $Li_4Ti_5O_{12}$ (pages 278–283) (/doi/10.1002/jrs.4999/full)

Dmitry V. Pelegov, Boris N. Slautin, Pavel S. Zelenovskiy, Dmitrii K. Kuznetsov, Evgeny A. Kiselev, Denis O. Alikin, Andrei L. Kholkin and Vladimir Ya. Shur

Version of Record online: 29 JUL 2016 | DOI: 10.1002/jrs.4999

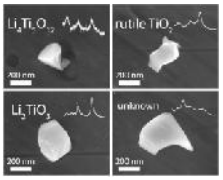

In this work we demonstrate that structural heterogeneity in a negative electrode material $Li_4Ti_5O_{12}$ with sub-micron grain size synthesized using standard solid-state method can be described locally via structural characterization of single particles using a combination of standard micro-Raman spectroscopy together with scanning electron microscopy. Proposed approach can be used for local structural characterization not only for $Li_4Ti_5O_{12}$, but also for a wide range of commercial products.

- Abstract (/doi/10.1002/jrs.4999/abstract)
- Article (/doi/10.1002/jrs.4999/full)
- PDF(392K) (/doi/10.1002/jrs.4999/epdf)
- PDF(392K) (/doi/10.1002/jrs.4999/pdf)
- References (/doi/10.1002/jrs.4999/full?scrollTo=references)
- Request Permissions (https://s100.copyright.com/AppDispatchServlet?publisherName=Wiley&publication=JRS&title=Single%20particle%20structure%20characterization%20of%20solid-state%20synthesized%20Li4Ti5O12&publicationDate=29%20JUL%202016&author=Dmitry%20V.%20Pelegov%2CBoris%20N.%20Slautin%2CPavel%20S.%20Zelenovskiy%2CDmitrii%20K.%20Kuznetsov%2CEvgeny%20A.%20Kiselev%2CDenis%20O.%20Alikin%2CAndrei%20L.%20Kholkin%2CVladimir%20Ya.%20Shur&startPage=278&endPage=283&copyright=Copyright%20%C2%A9%202016%20John%20Wiley%20%2526%20Sons%2C%20Ltd.&contentID=10.1002%2Fjrs.4999&orderSource=onlinelibrary%7Cwol1%7Ctoc&orderBeanReset=true)

19. Vibrational properties of β-$KSiH_3$ and β-$RbSiH_3$: a combined Raman and inelastic neutron scattering study (pages 284–291) (/doi/10.1002/jrs.5013/full)

Janos Mink, Yuan-Chih Lin, Maths Karlsson, Carin Österberg, Terrence J. Udovic, Henrik Fahlquist and Ulrich Häussermann

Version of Record online: 15 AUG 2016 | DOI: 10.1002/jrs.5013

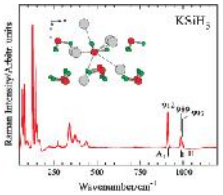

The recently identified hydrogen storage material $KSiH_3$ displays external modes at wavenumbers below 500 cm^{-1}. Raman spectroscopy is especially suitable for the analysis of the translations but allows also detection of well resolved libration modes of SiH_3^- anions in the region 300–450 cm^{-1}. With increasing temperature, libration bands broaden and redshift, indicating a significant softening.

- Abstract (/doi/10.1002/jrs.5013/abstract)
- Article (/doi/10.1002/jrs.5013/full)
- PDF(1872K) (/doi/10.1002/jrs.5013/epdf)
- PDF(1872K) (/doi/10.1002/jrs.5013/pdf)
- References (/doi/10.1002/jrs.5013/full?scrollTo=references)
- Request Permissions (https://s100.copyright.com/AppDispatchServlet?publisherName=Wiley&publication=JRS&title=Vibrational%20properties%20of%20%CE%B2-KSiH3%20and%20%CE%B2-RbSiH3%3A%20a%20combined%20Raman%20and%20inelastic%20neutron%20scattering%20study&publicationDate=15%20AUG%202016&author=Janos%20Mink%2CYuan-Chih%20Lin%2CMaths%20Karlsson%2CCarin%20%C3%96sterberg%2CTerrence%20J.%20Udovic%2CHenrik%20Fahlquist%2CUlrich%20H%C3%A4ussermann&startPage=284&endPage=291&copyright=Copyright%20%C2%A9%202016%20John%20Wiley%20%2526%20Sons%2C%20Ltd.&contentID=10.1002%2Fjrs.5013&orderSource=onlinelibrary%7Cwol1%7Ctoc&orderBeanReset=true)

20. Structural transformations in $Pb_{1-x}Bi_{4+x}Ti_{4-x}Mn_xO_{15}$ ($x = 0.2$ and 0.4): a Raman scattering study (pages 292–297) (/doi/10.1002/jrs.5030/full)

    Anton Prasetyo, Boriana Mihailova, Veinardi Suendo, A. A. Nugroho, Zulhadjri and Ismunandar

    Version of Record online: 23 SEP 2016 | DOI: 10.1002/jrs.5030

    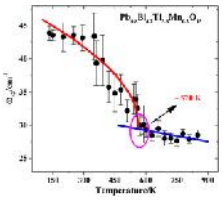

    The temperature evolution of phonon modes in four-layer Aurivillius-type $PbBi_4Ti_4O_{15}$ doped with Mn reveals structural transformations and chemistry-induced renormalization phenomena in this important class of magnetoelectric materials.

    - Abstract (/doi/10.1002/jrs.5030/abstract)
    - Article (/doi/10.1002/jrs.5030/full)
    - PDF(517K) (/doi/10.1002/jrs.5030/epdf)
    - PDF(517K) (/doi/10.1002/jrs.5030/pdf)
    - References (/doi/10.1002/jrs.5030/full?scrollTo=references)
    - Request Permissions (https://s100.copyright.com/AppDispatchServlet?publisherName=Wiley&publication=JRS&title=Structural%20transformations%20in%20Pb1%E2%80%89%E2%88%92%E2%80%89xBi4%E2%80%89%2B%E2%80%89xTi4%E2%80%89%E2%88%92%E2%80%89xMnxO15%20%28x%E2%80%89%3D%E2%80%890.2%20and%200.4%29%3A%20a%20Raman%20scattering%20study&publicationDate=23%20SEP%202016&author=Anton%20Prasetyo%2CBoriana%20Mihailova%2CVeinardi%20Suendo%2CA.%20A.%20Nugroho%2CZulhadjri%2CIsmunandar&startPage=292&endPage=297&copyright=Copyright%20%C2%A9%202016%20John%20Wiley%20%2526%20Sons%2C%20Ltd.&contentID=10.1002%2Fjrs.5030&orderSource=onlinelibrary%7Cwol1%7Ctoc&orderBeanReset=true)

21. *In-situ* high temperature Raman spectroscopic study on the structural evolution of $Na_2W_2O_7$ from the crystalline to molten states (pages 298–304) (/doi/10.1002/jrs.5036/full)

    J. Wang, J. L. You, A. A. Sobol, L. M. Lu, M. Wang, J. Wu, X. M. Lv and S. M. Wan

    Version of Record online: 21 SEP 2016 | DOI: 10.1002/jrs.5036

    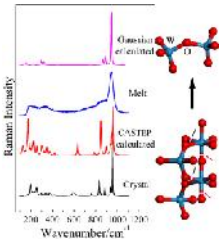

    The structural evolution of $Na_2W_2O_7$ from the crystalline to molten states, in particular, the microstructure of the melt formed, has been investigated by *in-situ* high temperature Raman spectroscopic technique and theoretical calculations. A new mechanism on the structural evolution of $Na_2W_2O_7$ during melting was proposed.

    - Abstract (/doi/10.1002/jrs.5036/abstract)
    - Article (/doi/10.1002/jrs.5036/full)
    - PDF(801K) (/doi/10.1002/jrs.5036/epdf)
    - PDF(801K) (/doi/10.1002/jrs.5036/pdf)
    - References (/doi/10.1002/jrs.5036/full?scrollTo=references)
    - Request Permissions (https://s100.copyright.com/AppDispatchServlet?publisherName=Wiley&publication=JRS&title=In-situ%20high%20temperature%20Raman%20spectroscopic%20study%20on%20the%20structural%20evolution%20of%20Na2W2O7%20from%20the%20crystalline%20to%20molten%20states&publicationDate=21%20SEP%202016&author=J.%20Wang%2CJ.%20L.%20You%2CA.%20A.%20Sobol%2CL.%20M.%20Lu%2CM.%20Wang%2CJ.%20Wu%2CX.%20M.%20Lv%2CS.%20M.%20Wan&startPage=298&endPage=304&copyright=Copyright%20%C2%A9%202016%20John%20Wiley%20%2526%20Sons%2C%20Ltd.&contentID=10.1002%2Fjrs.5036&orderSource=onlinelibrary%7Cwol1%7Ctoc&orderBeanReset=true)

22. Vibrational Raman optical activity of bicyclic terpenes: comparison between experimental and calculated vibrational Raman, Raman optical activity, and dimensionless circular intensity difference spectra and their similarity analysis (pages 305–313) (/doi/10.1002/jrs.5035/full)

    Prasad L. Polavarapu, Cody L. Covington, Katarzyna Chruszcz-Lipska, Grzegorz Zajac and Malgorzata Baranska

    Version of Record online: 21 SEP 2016 | DOI: 10.1002/jrs.5035

    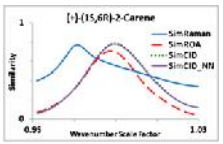

    Experimental and quantum chemical-predicted vibrational Raman optical activity (VROA) spectra of five terpenes are presented, and similarity between them is analyzed for Raman, VROA, and dimensionless circular intensity difference spectra. Simultaneous analysis of VROA and circular intensity difference spectra is shown to be more useful than restricting the analysis to VROA alone. Anisotropic contributions arising from electric dipole-electric quadrupole polarizability are shown to smaller than those from electric dipole-magnetic dipole polarizability.

    - Abstract (/doi/10.1002/jrs.5035/abstract)
    - Article (/doi/10.1002/jrs.5035/full)
    - PDF(1222K) (/doi/10.1002/jrs.5035/epdf)
    - PDF(1222K) (/doi/10.1002/jrs.5035/pdf)
    - References (/doi/10.1002/jrs.5035/full?scrollTo=references)
    - Request Permissions (https://s100.copyright.com/AppDispatchServlet?publisherName=Wiley&publication=JRS&title=Vibrational%20Raman%20optical%20activity%20of%20bicyclic%20terpenes%3A%20comparison%20between%20experimental%20and%20calculated%20vibrational%20Raman%2C%20Raman%20optical%20activity%2C%20and%20dimensionless%20circular%20intensity%20difference%20spectra%20and%20their%20similarity%20analysis&publicationDate=21%20SEP%202016&author=Prasad%20L.%20Polavarapu%2CCody%20L.%20Covington%2CKatarzyna%20Chruszcz-Lipska%2CGrzegorz%20Zajac%2CMalgorzata%20Baranska&startPage=305&endPage=313&copyright=Copyright%20%C2%A9%202016%20John%20Wiley%20%2526%20Sons%2C%20Ltd.&contentID=10.1002%2Fjrs.5035&orderSource=onlinelibrary%7Cwol1%7Ctoc&orderBeanReset=true)

23. Temperature and salinity effects on the Raman scattering cross section of the water OH-stretching vibration band in NaCl aqueous solutions from 0 to 300 °C (pages 314–322) (/doi/10.1002/jrs.5039/full)

    Xiangen Wu, Wanjun Lu, Wenjia Ou, Marie-Camille Caumon and Jean Dubessy

    Version of Record online: 21 SEP 2016 | DOI: 10.1002/jrs.5039

    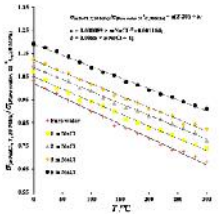

    The relative Raman scattering cross section (RSCS) of the OH-stretching vibration band of liquid water ($\sigma_{(m\text{NaCl},\ T,\ 30\ \text{MPa})}/\sigma_{(\textit{Pure water},\ 20^{\circ}\text{C},\ 30\ \text{MPa})}$) as a function of temperature (T, in °C) and salinity (mNaCl, in mol/kg · H_2O) was established. The relative RSCS of water OH band decreases linearly with increasing temperature and increases with increasing NaCl concentration. The enhancement effect of NaCl increases with rising temperature.

    - Abstract (/doi/10.1002/jrs.5039/abstract)
    - Article (/doi/10.1002/jrs.5039/full)
    - PDF(464K) (/doi/10.1002/jrs.5039/epdf)
    - PDF(464K) (/doi/10.1002/jrs.5039/pdf)
    - References (/doi/10.1002/jrs.5039/full?scrollTo=references)
    - Request Permissions (https://s100.copyright.com/AppDispatchServlet?publisherName=Wiley&publication=JRS&title=Temperature%20and%20salinity%20effects%20on%20the%20Raman%20scattering%20cross%20section%20of%20the%20water%20OH-

stretching%20vibration%20band%20in%20NaCl%20aqueous%20solutions%20from%200%20to%20300%E2%80%89C%2B0C&publicationDate=21%20SEP%202016&author=Xiangen%20Wu%2CWanjun%20Lu%2CWenjia%20Ou%2CMarie-Camille%20Caumon%2CJean%20Dubessy&startPage=314&endPage=322&copyright=Copyright%20%C2%A9%202016%20John%20Wiley%20%2526%20Sons%2C%20Ltd.&contentID=10.1002%2Fjrs.5039&orderSource=onlinelibrary%7Cwol1%7Ctoc&orderBeanReset=true)

24. How the vibrational frequency varies with temperature (pages 323–326) (/doi/10.1002/jrs.5009/full)

    Boris A. Kolesov

    Version of Record online: 10 AUG 2016 | DOI: 10.1002/jrs.5009

    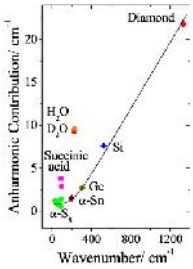

    A changing of mode wavenumber with temperature is described by a simple, understandable and realistic approach. The fitting of ω(*T*) function in the spectra of diamond, silicon and α-S_8 molecular crystal is presented. Anharmonic contributions from vibrations of different types of chemical bonds are considered. Anharmonicity of hydrogen bonds is essentially higher than that of the other types of chemical bond.

    - Abstract (/doi/10.1002/jrs.5009/abstract)
    - Article (/doi/10.1002/jrs.5009/full)
    - PDF(269K) (/doi/10.1002/jrs.5009/epdf)
    - PDF(269K) (/doi/10.1002/jrs.5009/pdf)
    - References (/doi/10.1002/jrs.5009/full?scrollTo=references)
    - Request Permissions (https://s100.copyright.com/AppDispatchServlet?publisherName=Wiley&publication=JRS&title=How%20the%20vibrational%20frequency%20varies%20with%20temperature&publicationDate=10%20AUG%202016&author=Boris%20A.%20Kolesov&startPage=323&endPage=326&copyright=Copyright%20%C2%A9%202016%20John%20Wiley%20%2526%20Sons%2C%20Ltd.&contentID=10.1002%2Fjrs.5009&orderSource=onlinelibrary%7Cwol1%7Ctoc&orderBeanReset=true)

25. PICVib: an accurate, fast and simple procedure to investigate selected vibrational modes at high theoretical levels and evaluate Raman intensities (pages 327–335) (/doi/10.1002/jrs.5008/full)

    Marcus V. P. dos Santos, Yaicel G. Proenza, Ayyaz Mahmood and Ricardo L. Longo

    Version of Record online: 9 AUG 2016 | DOI: 10.1002/jrs.5008

    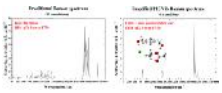

    PICVib has become a complete, fast, and accurate tool for (harmonic) vibrational spectra predictions (wavenumbers, Raman, and infrared intensities) at high computational levels.

    - Abstract (/doi/10.1002/jrs.5008/abstract)
    - Article (/doi/10.1002/jrs.5008/full)
    - PDF(375K) (/doi/10.1002/jrs.5008/epdf)
    - PDF(375K) (/doi/10.1002/jrs.5008/pdf)
    - References (/doi/10.1002/jrs.5008/full?scrollTo=references)
    - Request Permissions (https://s100.copyright.com/AppDispatchServlet?publisherName=Wiley&publication=JRS&title=PICVib%3A%20an%20accurate%2C%20fast%20and%20simple%20procedure%20to%20investigate%20selected%20vibrational%20modes%20at%20high%20theoretical%20levels%20and%20evaluate%20Raman%20intensities&publicationDate=09%20AUG%202016&author=Marcus%20V.%20P.%20Santos%2CYaicel%20G.%20Proenza%2CAyyaz%20Mahmood%2CRicardo%20L.%20Longo&startPage=327&endPage=335&copyright=Copyright%20%C2%A9%202016%20John%20Wiley%20%2526%20Sons%2C%20Ltd.&contentID=10.1002%2Fjrs.5008&orderSource=onlinelibrary%7Cwol1%7Ctoc&orderBeanReset=true)

26. Iterative morphological and mollifier-based baseline correction for Raman spectra (pages 336–342) (/doi/10.1002/jrs.5010/full)

    Matthias Koch, Christian Suhr, Bernhard Roth and Merve Meinhardt-Wollweber

    Version of Record online: 8 AUG 2016 | DOI: 10.1002/jrs.5010

    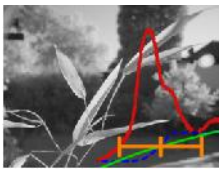

    A new baseline correction algorithm has been developed which is especially suited for strong fluorescent and irregularly shaped baselines which are common for *in vivo* Resonance Raman measurements. Our iterative algorithm, which employs a morphological operator in combination with mollification, will be described and application examples for both continuous wave and widely tunable excitation-emission-map spectra will be shown.

    - Abstract (/doi/10.1002/jrs.5010/abstract)
    - Article (/doi/10.1002/jrs.5010/full)
    - PDF(654K) (/doi/10.1002/jrs.5010/epdf)
    - PDF(654K) (/doi/10.1002/jrs.5010/pdf)
    - References (/doi/10.1002/jrs.5010/full?scrollTo=references)
    - Request Permissions (https://s100.copyright.com/AppDispatchServlet?publisherName=Wiley&publication=JRS&title=Iterative%20morphological%20and%20mollifier-based%20baseline%20correction%20for%20Raman%20spectra&publicationDate=08%20AUG%202016&author=Matthias%20Koch%2CChristian%20Suhr%2CBernhard%20Roth%2CMerve%20Meinhardt-Wollweber&startPage=336&endPage=342&copyright=Copyright%20%C2%A9%202016%20John%20Wiley%20%2526%20Sons%2C%20Ltd.&contentID=10.1002%2Fjrs.5010&orderSource=onlinelibrary%7Cwol1%7Ctoc&orderBeanReset=true)

3. **Short communication**

1. Top of page
2. Issue information
3. Research articles
4. Short communication

1. Two different behaviors in 4-ABT and 4,4′-DMAB surface enhanced Raman spectroscopy (pages 343–347) (/doi/10.1002/jrs.5016/full)

    Dongha Shin

    Version of Record online: 14 SEP 2016 | DOI: 10.1002/jrs.5016

    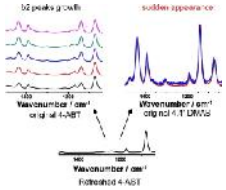

    Borohydride treated-refreshed 4-ABT, which has no b2-type bands, shows gradual increase of b2-type bands at original 4-ABT side while abrupt appearance of b2-type bands at original 4,4′-DMAB side during laser irradiation.

    - Abstract (/doi/10.1002/jrs.5016/abstract)
    - Article (/doi/10.1002/jrs.5016/full)
    - PDF(405K) (/doi/10.1002/jrs.5016/epdf)
    - PDF(405K) (/doi/10.1002/jrs.5016/pdf)
    - References (/doi/10.1002/jrs.5016/full?scrollTo=references)
    - Request Permissions (https://s100.copyright.com/AppDispatchServlet?publisherName=Wiley&publication=JRS&title=Two%20different%20behaviors%20in%204-ABT%20and%204%2C4%E2%80%B2-DMAB%20surface%20enhanced%20Raman%20spectroscopy&publicationDate=14%20SEP%202016&author=Dongha%20Shin&startPage=343&endPage=347&copyright=Copyright%20%C2%A9%202016%20John%20Wiley%20%2526%20Sons

Research article

Journal of RAMAN SPECTROSCOPY

Received: 21 May 2016 Revised: 15 August 2016 Accepted: 19 August 2016 Published online in Wiley Online Library: 23 September 2016

(wileyonlinelibrary.com) DOI 10.1002/jrs.5030

Structural transformations in $Pb_{1-x}Bi_{4+x}Ti_{4-x}Mn_xO_{15}$ (x=0.2 and 0.4): a Raman scattering study

Anton Prasetyo,[a,b]* Boriana Mihailova,[c] Veinardi Suendo,[a,d] A. A. Nugroho,[e] Zulhadjri[f] and Ismunandar[a]*

The temperature evolution of the Raman scattering of $Pb_{1-x}Bi_{4+x}Ti_{4-x}Mn_xO_{15}$ (x = 0.2 and 0.4) on cooling from 850 to 140–130 K was studied in order to elucidate the effect of *B*-site Mn^{3+} doping accompanied by the increase in the *A*-site Bi^{3+} content on the structural transformations in four-layer Aurivillius-type compound ($A_{n-1}Bi_2B_nO_{3n+3}$, n = 4). The ferroelectric–paraelectric transition (T_c ~800 K for x = 0.2 and ~765 K for x = 0.4) is well mirrored by the Raman scattering near 60 cm^{-1} arising from the so-called rigid layer mode. The temperature dependence of the phonon mode near 42 cm^{-1} arising from *A*-site Pb/Bi displacements indicates a second structural transformation near 570 K and 400 K for x = 0.2 and 0.4, respectively, similar to that observed for Mn-free $PbBi_4Ti_4O_{15}$. This structural alteration resembles a thermodynamically second-order phase transition for all three compounds and the critical temperature (T_a) decreases with the increase in the *A*-site Bi^{3+} amount, related to the heterovalent substitution (Mn^{3+} for Ti^{4+}) on the *B* site; T_a = 600, 570, 400 K for x = 0, 0.2, 0.4, respectively. The BO_6 tilting and bending mode near 220 cm^{-1} also shows an anomaly at T_a, and, thus, this second structural transformation was attributed to subtle rearrangements of *A*-site cations accompanied by octahedral BO_6 tilting in the perovskite-like blocks. Copyright © 2016 John Wiley & Sons, Ltd.

Keywords: Aurivillius structure-type; ferroelectric phase transition; phonon modes; temperature dependence

Introduction

The world of ferroelectrics is dominated by the perovskite-type materials, but the quest to find environmentally friendly multifunctional materials with a reduced or none content of Pb has led to renewed interest of alternative structure types. Thus, materials of the Aurivillius structure type have been attracted much of attention in recent years because of their sufficiently good dielectric properties and high ferroelectric (FE)–paraelectric (PE) phase transition temperature as well as because of the appearance of magnetism upon appropriate doping.[1–9] Magnetoelectric materials have the advantage to combine magnetic and ferroelectric properties and therefore show a great potential to be used for information storage.[10–12] The general formula of Aurivillius-type compounds is $(Bi_2O_2)^{2+}(A_{n-1}B_nO_{3n+1})^{2-}$, where the *A* site is occupied by large cations such as Ca^{2+}, Sr^{2+}, Ba^{2+}, Pb^{2+}, Bi^{3+}, Na^+ or a mixture of these cations, and the *B* site is occupied by smaller cations with a higher charge such as Fe^{3+}, Cr^{3+},Ti^{4+}, Nb^{5+}, Ta^{5+}, W^{6+} or Mo^{6+}. The structure consists of fluorite-like blocks and perovskite-like blocks, as n is an integer representing the number of perovskite-like blocks.[13,14] The ferroelectric properties of Aurivillius compounds have been discovered by Smolenskii *et al*. in 1959.[15] The ferroelectricity in Aurivillius compounds stems from several mechanisms: (1) the displacive mechanism, which involves *A*-site and/or *B*-site cationic displacements, (2) the rigid layer (RL) mode which involved displacements of the Bi_2O_2 fluorite-like planes relative to the perovskite-like blocks, and (3) the octahedral tilting in perovskite-like blocks.[16–18] Magnetic properties may arise by incorporating magnetically active cations such as Fe^{3+}, Mn^{3+} into the *B* site in the perovskite blocks.[1–6,8,19–23]

$Pb_{1-x}Bi_{4+x}Ti_{4-x}Mn_xO_{15}$ (x = 0.2 and 0.4) are members of the four-layer Aurivillius family which was first synthesized by Zulhadjri *et al*. (2011) using the molten salt method. Both compounds have a space group $A2_1am$ with unit-cell parameters a = 5.4509(4) Å, b = 5.4304(3) Å and c = 41.340(2) Å for $Pb_{0.8}Bi_{4.2}Ti_{3.8}Mn_{0.2}O_{15}$, and

* *Correspondence to: Ismunandar, Inorganic and Physical Chemistry Research Division, Faculty Mathematics and Natural Sciences, Institut Teknologi Bandung, Jl. Ganesha 10, Bandung 40132, Indonesia.*
E-mail: ismu@chem.itb.ac.id

* *Correspondence to: Anton Prasetyo, Department of Chemistry, UIN Maulana Malik Ibrahim, Jl. Gajayana 50, Malang 65144, Indonesia.*
E-mail: antoniaprasetyo@gmail.com

a *Physical and Inorganic Chemistry Research Group, Faculty Mathematics and Natural Sciences, Institut Teknologi Bandung, Jl. Ganesha 10, Bandung 40132, Indonesia*

b *Department of Chemistry, UIN Maulana Malik Ibrahim, Jl. Gajayana 50, Malang 65144, Indonesia*

c *Department Geowissenschaften, Universität Hamburg, Grindelallee 48, Hamburg 20146, Germany*

d *Research Center For Nanosciences And Nanotechnology, Institut Teknologi Bandung, Jl. Ganesha 10, Bandung 40132, Indonesia*

e *Physics of Magnetism and Photonic Research Division, Faculty Mathematics and Natural Sciences, Institut Teknologi Bandung, Jl. Ganesha 10, Bandung 40132, Indonesia*

f *Department of Chemistry, Faculty of Mathematics and Natural Sciences, Universitas Andalas, Kampus Limau Manis, Padang 25163, Indonesia*

$a = 5.4420(4)$ Å, $b = 5.4258(3)$ Å and $c = 41.185(3)$ Å for $Pb_{0.6}Bi_{4.4}Ti_{3.6}Mn_{0.4}O_{15}$. The temperature dependence of the dielectric permittivity reveals a FE–PE phase transition temperature at 803 K for $Pb_{0.8}Bi_{4.2}Ti_{3.8}Mn_{0.2}O_{15}$ and at 813 K for $Pb_{0.6}Bi_{4.4}Ti_{3.6}Mn_{0.4}O_{15}$. The introduction of Mn^{3+} dopant results in paramagnetic behavior, and thus $Pb_{1-x}Bi_{4+x}Ti_{4-x}Mn_xO_{15}$ ($x = 0.2$ and 0.4) can be classified as magnetoelectric material.[8]

To better understand how properties can be tuned via chemistry, fundamental studies of the relation composition–structure–properties are required. Hence, a deeper knowledge on how the substitution disorder influences the structure and transformation processes of the host matrix is needed. Raman spectroscopy is a very appropriate method for studying ferroic phase transitions as well as subtle structural transformations, even if they take place only on a mesoscopic length scale. The structural alterations driven by the temperature decrease modify the phonon density of states, and thus the critical/characteristic temperatures can be deduced from the appearance of new peaks as well as from anomalies in the temperature dependencies of the positions, widths and integrated intensities of the pre-existing Raman peaks.[24–29] In our recent work, we investigated the temperature-dependent Raman spectra of $PbBi_4Ti_4O_{15}$ and found that there are three structural transformations near 400, 600 and 800 K.[18] The structural transformation at ~800 K is driven by the RL mode near 60 cm^{-1} and corresponds to the FE–PE transition. Additional anomaly in the RL mode was found at 400 K, which, however, should not be related to changes in the ferroelectric properties, because no anomaly in the dielectric permittivity was observed.[8] The structural transformation at 600 K is mirrored by the phonon mode near 40 cm^{-1}, attributed to *A*-site Pb/Bi displacements, as well as to the phonon mode near 220 cm^{-1}, assigned to octahedral tilting and bending.[18] This structural alteration corresponds well to the minor change in the spontaneous polarization observed at 600 K,[8] and according to the temperature dependence of the phonon mode near 40 cm^{-1}, it resembles the behavior of a second-order phase transition.[18] Trivalent Mn partially substitutes for Ti^{4+} at the *B* site in the perovskite blocks, which for charge-balancing reasons leads to a partial substitution of Bi^{3+} for Pb^{2+} at the *A* site.[8] Neutron diffraction analyses of $Pb_{1-x}Bi_{4+x}Ti_{4-x}Mn_xO_{15}$ ($x = 0.2$ and 0.4) showed that Mn^{3+} influences mainly the local structure of TiO_6, in particular the Ti—O bond lengths. Zulhadjri *et al.*[8] also demonstrated that the FE–PE transition temperature T_c of $Pb_{0.6}Bi_{4.4}Ti_{3.6}Mn_{0.4}O_{15}$ is with ~10 K higher than that of $Pb_{0.8}Bi_{4.2}Ti_{3.8}Mn_{0.2}O_{15}$. The slight increase in T_c was ascribed to the fact that for $x \leq 0.2$ the net polarization is predominantly related to the inner-layer Ti(1)O_6, whereas for $x > 0.2$ to the outer most-layer Ti(2)O_6 because the average dipole moment of the latter type of octahedral increases mainly along the *a* axis with increasing Mn^{3+} doping. In the present work, the effect of *B*-site Mn^{3+} doping and the accompanied decrease of *A*-site Pb^{2+} on the structural transformation are studied by *in situ* temperature-dependent Raman spectroscopy of $Pb_{1-x}Bi_{4+x}Ti_{4-x}Mn_xO_{15}$ ($x = 0.2$ and 0.4) in the range 120–850 K, to further elucidate the temperature-driven transformation processes in the $PbBi_4Ti_4O_{15}$ family.

Experiment

Polycrystalline Mn^{3+}-doped $PbBi_4Ti_4O_{15}$ compounds were synthesized by the molten salt method reported by Zulhadjri *et al.*[8] Trivalent Mn in the form of Mn_2O_3 was used in the reactant mixture, and the performed Rietveld refinements to powder diffraction data on $Pb_{1-x}Bi_{4+x}Ti_{4-x}Mn_xO_{15}$ with $x = 0.2$ and 0.4 revealed a chemical composition of the final product that corresponds to trivalent Mn.

Raman spectra were obtained using a Horiba Jobin-Yvon T64000 triple-monochromator Raman spectrometer equipped with an Olympus BH41 microscope. The spectra were measured in the range 15–1215 cm^{-1} with spectral resolution ~2 cm^{-1}. The Raman scattering was excited with the 514-nm line of an Ar^+ laser. Data were measured in the spectral range 15–1215 cm^{-1} with a spectral resolution ~2 cm^{-1}. The spectra were collected on plate-shaped pellets in a backscattering geometry. It should be mentioned that if the mean grain size approaches a few unit cells, that is, ~25 nm in the case of Aurivillius-type compounds, elastic strains in the vicinity of grain boundaries might lead to detectable effects on the temperature evolution of phonon modes. However, the sharpness of the Bragg diffraction peaks (see Ref.[8]) indicates that the average grain size in the compounds studied here is well beyond this limit. At the same time, at room temperature, no polarization, orientation or spatial dependence of the Raman spectra was detected, indicating that the average linear crystallite size is small enough as compared to the diameter of the laser spot on the sample surface, which was ca. 2 microns, to ensure homogeneity of the polycrystalline samples with respect to the Raman scattering they produce.

The spectra were collected on cooling from 850 to 120 K with a step of 30 K, except for the range from 600 to 550 K where a finer step size of 10 K was used, in a Linkam TM600E heating/cooling stage. The reversibility of the observed temperature-induced structural changes was verified by measuring the room-temperature spectrum at the end of each run.

The spectra were reduced by the Bose–Einstein occupation factor to eliminate the conventional effect of temperature on spectral intensities.[30] A Lorentzian model was used to fit Raman spectra and to obtained the peak positions, full widths at half maximum (FWHMs) and integrated intensities.

Results and discussion

The structure of $Pb_{1-x}Bi_{4+x}Ti_{4-x}Mn_xO_{15}$ ($x = 0.2$ and 0.4) has a space group $A2_1am$, and therefore according to group theory, there are 141 Raman-active modes: $36A_1 + 35A_2 + 34B_1 + 36B_2$.[31] However, a smaller number of resolved peaks are experimentally observed at all temperatures, because of peak overlapping and/or very weak intensities. Hence, for each compound, we first fitted the spectrum measured at the lowest temperature, and the number of included peaks was chosen so that $dI/I < 1$ for all peaks, where *I* and *dI* are the calculated integrated intensity and the corresponding uncertainty.[32] Then, the same number of peaks was used as a starting model for the spectrum measured at the next higher temperature, and if for a certain peak $dI/I \geq 1$, that peak was removed. Figure 1 shows the low-temperature Raman spectra of $Pb_{1-x}Bi_{4+x}Ti_{4-x}Mn_xO_{15}$ with $x = 0$, 0.2 and 0.4 collected at 120, 133 and 148 K respectively, along with the fitting Lorentzian functions for $x = 0$. As can be seen in Fig. 1, the overall Raman scattering of both Mn-containing compounds is similar to that of Mn-free $PbBi_4Ti_4O_{15}$, but the peak positions are slightly different, which is caused by the substitution-induced changes in the local structure. The partial replacement of Ti by Mn at the octahedral centers changes the mean *B*—O bond length and consequently affects the peak positions of the internal TiO_6 modes (>200 cm^{-1}), while the substitution of Pb by Bi affects mainly the external TiO_6 modes (<200 cm^{-1}). The

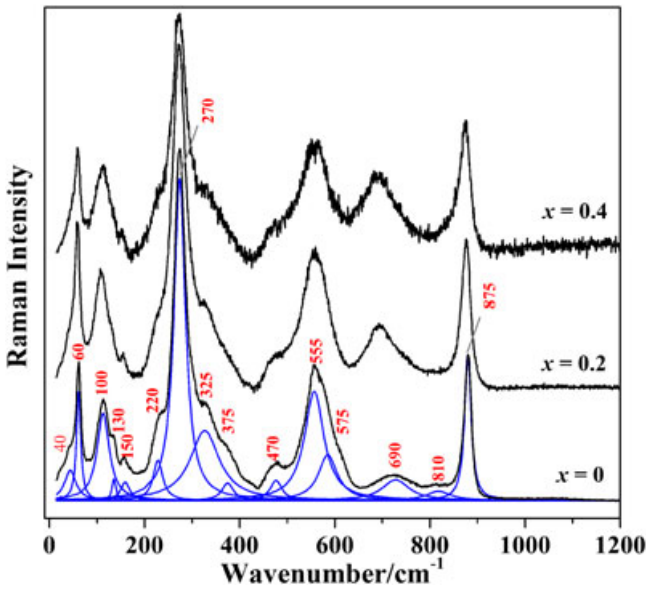

Figure 1. Raman spectra of $Pb_{1-x}Bi_{4+x}Ti_{4-x}Mn_xO_{15}$ with $x = 0$, 0.2 and 0.4 collected at 120, 133 and 148 K, respectively, along with the fitting Lorentzian functions for $x = 0$.

assignment of the Raman-active phonon modes in Aurivillius compounds based on previous studies is given in Table 1.

Figure 2 shows the Raman spectra of $Pb_{0.8}Bi_{4.2}Ti_{3.8}Mn_{0.2}O_{15}$ and $Pb_{0.6}Bi_{4.4}Ti_{3.6}Mn_{0.4}O_{15}$ at selected temperatures in the range 130–850 K. The corresponding temperature dependencies of the wavenumber of the mode ~42 cm^{-1} involving *A*-site Pb^{2+}/Bi^{3+} displacements are depicted in Fig. 3. Withers *et al.* suggested that for Aurivillius compounds with a space group $A2_1am$, the displacements of the *A*-site cations in the perovskite blocks are strongly related to the major spontaneous polarization.[16] Previous Raman spectroscopic studies on the nature of ferroelectricity in Aurivillius compounds have also demonstrated the interplay between the *A*-site cationic displacements and the FE–PE phase transition.[25,33,47–49] As can be seen in Fig. 3, $\omega_{42}(T)$ for both Mn-doped compounds shows the same behavior as for Mn-free $PbBi_4Ti_4O_{15}$.[18] Fits to the low-temperature data points by a Landau-type power function $\omega = \mu(T_c - T)^{\beta}$ reveal a structural transformations at T_a ~570 K for $Pb_{0.8}Bi_{4.2}Ti_{3.8}Mn_{0.2}O_{15}$ and ~400 K for $Pb_{0.6}Bi_{4.4}Ti_{3.6}Mn_{0.4}O_{15}$. This intermediate structural transformation occurs at $T_a \sim 600$ K for pure $PbBi_4Ti_4O_{15}$ as revealed by Raman spectroscopy,[18] and it corresponds well to the anomaly in the temperature dependence of dielectric permittivity observed for

Table 1. Assignment of Raman-active phonon modes of $Pb_{1-x}Bi_{4+x}Ti_{4-x}Mn_xO_{15}$ ($x = 0$, 0.2 and 0.4)

Peak position (cm^{-1})	Assignment
~42	*A*-site cation displacement [33–36]
~60	Rigid layer (*RL*) mode [33,37,38]
~100, 130, 150	Translational modes of *A*-site and *B*-site cations [39–43]
~220, 270	BO_6 bending and tilting [33,44,45]
~325, 375	The combination of BO_6 bending–stretching and tilting [37,38,44]
~470	BO_6 torsional mode [45]
~555, 690	BO_6 stretching modes [37,38]
~870	Symmetric BO_6 stretching [45,46]

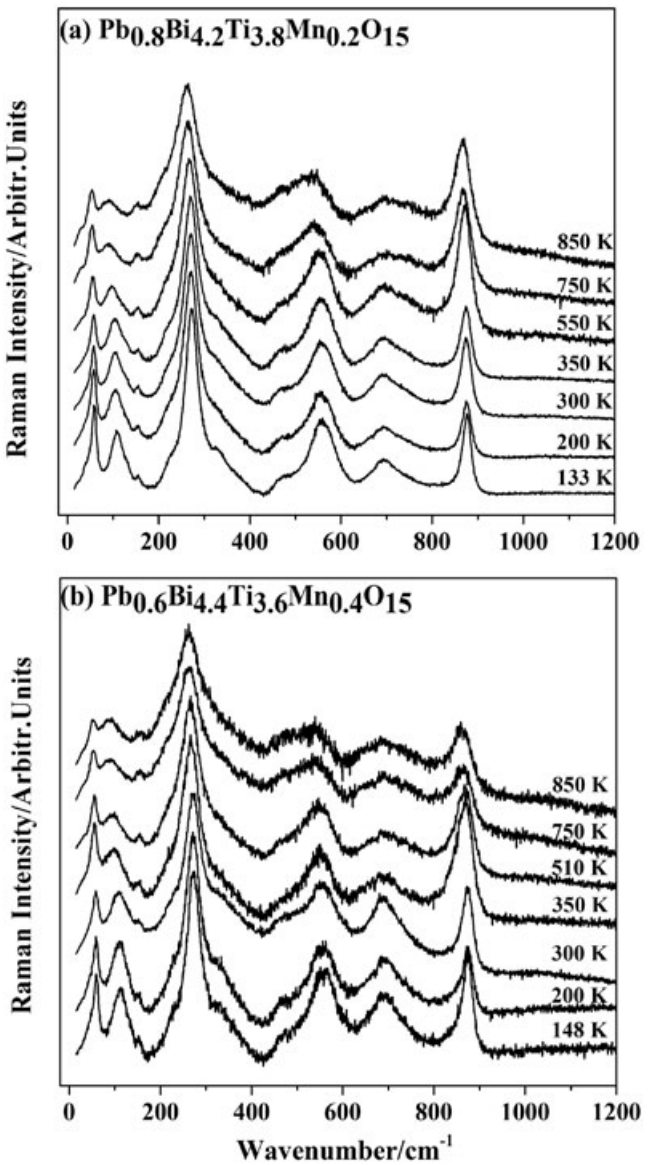

Figure 2. Raman spectra at selected temperatures between 130 and 850 K for (a) $Pb_{0.8}Bi_{4.2}Ti_{3.8}Mn_{0.2}O_{15}$, and (b) $Pb_{0.6}Bi_{4.4}Ti_{3.6}Mn_{0.4}O_{15}$.

$x = 0$. X-ray diffraction analysis also revealed the occurrence of T_a in $ABi_4Ti_4O_{15}$ with $A = Pb$,[50] and it was suggested that the subtle changes in the $PbBi_4Ti_4O_{15}$ structure at 600 K are because of the influence of Pb^{2+} cations on the BO_6 octahedral tilting.[50] It should be noted that a similar intermediate structural transformation near 510 K was reported for $SrBi_2Ta_2O_9$ and $Sr_{0.85}Bi_{2.1}Ta_2O_9$ based on Rietveld refinements to X-ray diffraction data.[51,52] Hence, this intermediate transformation seems to be characteristic of all Aurivillius-type materials, and, as indicated by our results, its characteristic temperature T_a depends on the chemistry at the B site of the perovskite-like block. The value of the critical exponential β obtained from the Raman data presented here can be used to estimate the type of phase transition.[53] For all three compounds ($x = 0$, 0.2, 0.4), β is close to 0.5, suggesting a thermodynamically second-order structural transformation. The fitting results are given in Table 2. The R^2-value of $Pb_{0.6}Bi_{4.4}Ti_{3.6}Mn_{0.4}O_{15}$ is poor because of the large uncertainties of ω_{42} in the temperature range 350–450 K.

In our previous work on $PbBi_4Ti_4O_{15}$, we found that the temperature dependence of the wavenumber of the RL mode (ω_{60}) clearly

Journal of RAMAN SPECTROSCOPY

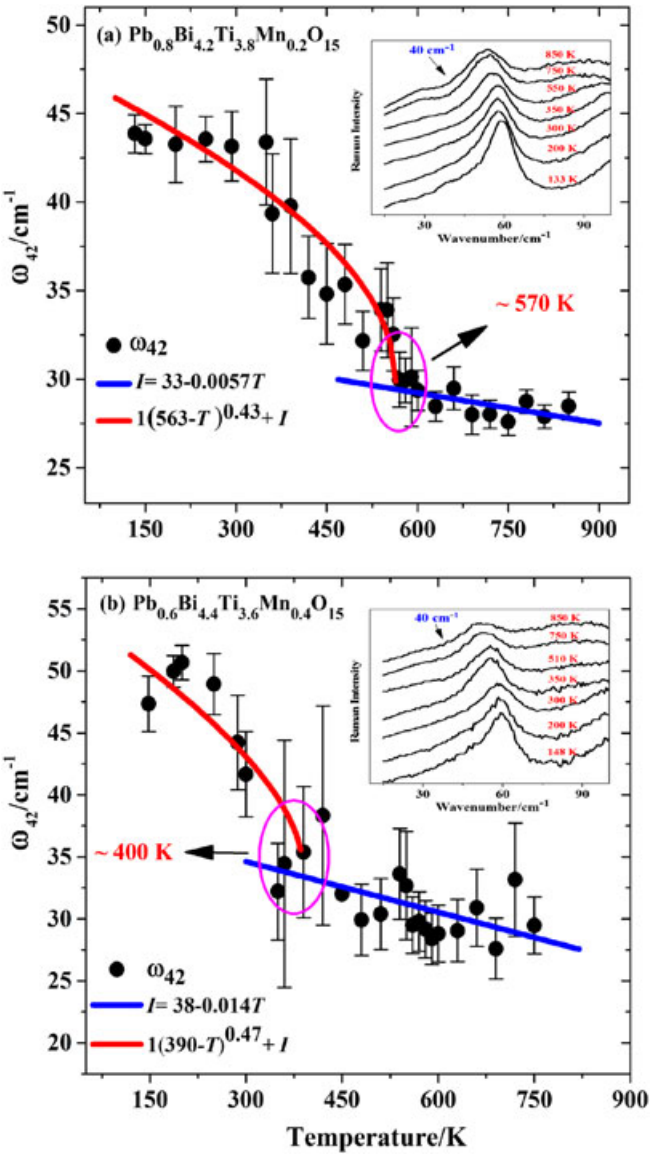

Figure 3. Temperature dependence of the wavenumber of the phonon mode near 42 cm^{-1}: (a) $Pb_{0.8}Bi_{4.2}Ti_{3.8}Mn_{0.2}O_{15}$, and (b) $Pb_{0.6}Bi_{4.4}Ti_{3.6}Mn_{0.4}O_{15}$. The ellipse indicates the anomaly. The blue lines represent linear fits to the data points above 570 for $Pb_{0.8}Bi_{4.2}Ti_{3.8}Mn_{0.2}O_{15}$ and 400 K for $Pb_{0.6}Bi_{4.4}Ti_{3.6}Mn_{0.4}O_{15}$, while the red lines fits to the data point below 570/400 K with a Landau-type power function $\omega = \mu(Tc - T)\beta$. The insets show the low-wavenumber Raman spectra of $Pb_{0.8}Bi_{4.2}Ti_{3.8}Mn_{0.2}O_{15}$, and $Pb_{0.6}Bi_{4.4}Ti_{3.6}Mn_{0.4}O_{15}$ at selected temperature.

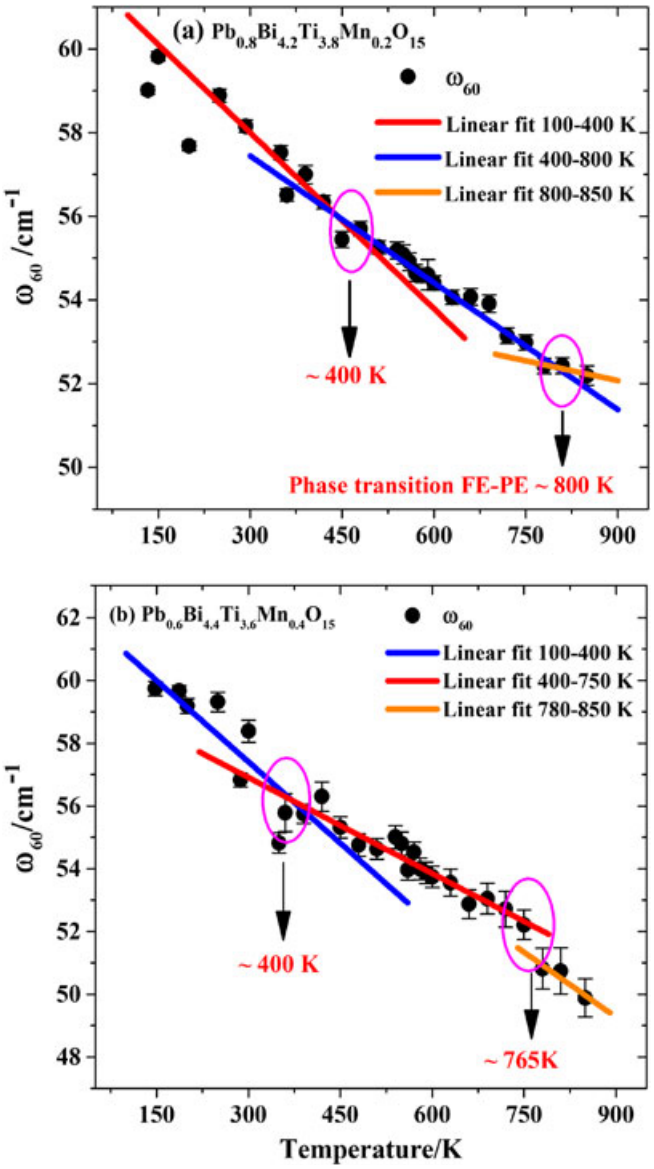

Figure 4. Temperature dependence of the wavenumber of the phonon mode near 60 cm^{-1}: (a) $Pb_{0.8}Bi_{4.2}Ti_{3.8}Mn_{0.2}O_{15}$ (ellipses indicate the anomalies near 400 and 800 K), and (b) $Pb_{0.6}Bi_{4.4}Ti_{3.6}Mn_{0.4}O_{15}$ (ellipses indicate the anomalies near 400 and 765 K).

Table 2. The result of Landau-type power function fitting of $\omega_{40}(T)$ for $Pb_{1-x}Bi_{4+x}Ti_{4-x}Mn_xO_{15}$ ($x = 0$, 0.2 and 0.4)

Compound	T_a (K)	β	R^2
$x = 0$ [18]	591 ± 5	0.46 ± 0.06	0.86
$x = 0.2$	563 ± 13	0.43 ± 0.11	0.83
$x = 0.4$	390 ± 10	0.47 ± 0.3	0.59

reveals the PE–FE phase transition as well as additional structural changes near 400 K, which are not related to the ferroelectric properties.[18] As can be seen in Fig. 4, the RL mode in both Mn-doped samples exhibits a similar trend. The higher-temperature kink in $\omega_{60}(T)$ is around 800 K for $x = 0.2$, which matches well the corresponding PE–FE phase transition temperature at 803 K revealed by the maximum of the dielectric permittivity as a function of temperature[8] For $x = 0.4$, $\omega_{60}(T)$ exhibits a small but clear abrupt jump between 750 and 780 K, which should correspond to the Curie temperature. The discontinuity in $\omega_{60}(T)$ occurs slightly below the temperature of the dielectric-permittivity maximum $T_m = 813$ K for $Pb_{0.6}Bi_{4.4}Ti_{3.6}Mn_{0.4}O_{15}$,[8] which might be because of doping-induced diffuseness of the FE–PE phase transition and the difference in the sensitivity of the two methods. Therefore, the driving mechanism of formation of ferroelectricity for all three compounds $Pb_{1-x}Bi_{4+x}Ti_{4-x}Mn_xO_{15}$ ($x = 0$, 0.2 and 0.4) is the RL mode, as suggested by Stachiotti *et al.* (2000).[17] Interestingly, the lower-temperature kink of $\omega_{60}(T)$ appears near 400 K for $x = 0$, 0.2 and 0.4, indicating that Mn doping negligibly influences this structural alteration near 400 K. For $x = 0$, a subtle change near 400 K can be observed also in the temperature dependence of $\omega_{40}(T)$, and it was attributed to a non-polar structural alteration involving

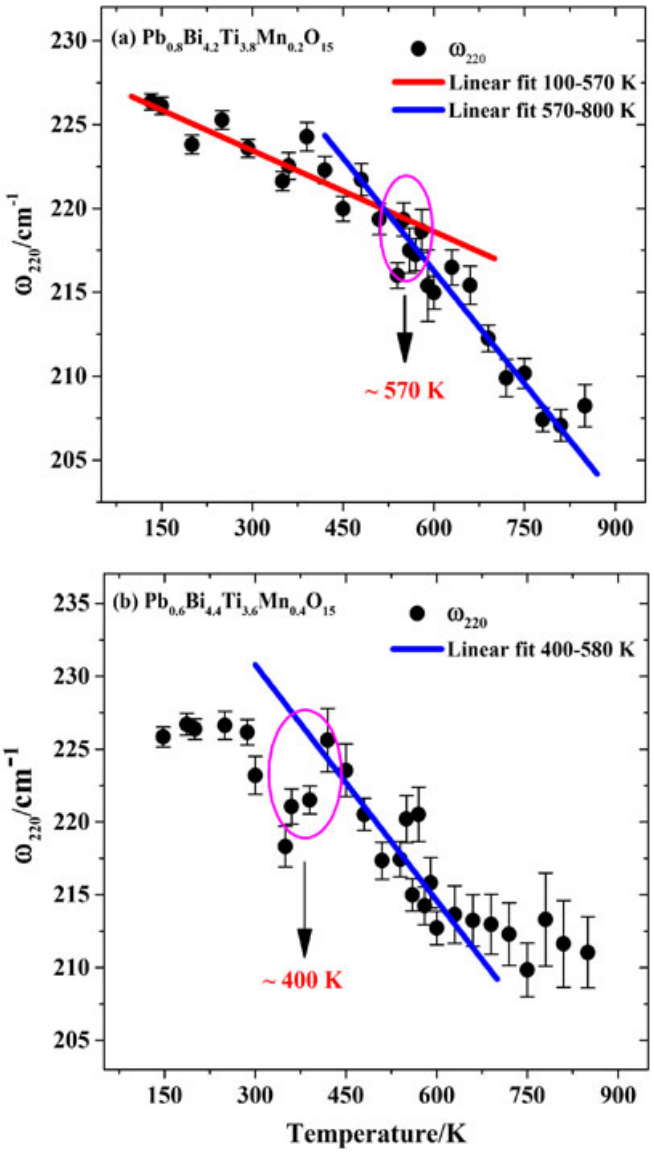

Figure 5. Temperature dependence of the wavenumber of the phonon mode near 220 cm^{-1}: (a) $Pb_{0.8}Bi_{4.2}Ti_{3.8}Mn_{0.2}O_{15}$, and (b) $Pb_{0.6}Bi_{4.4}Ti_{3.6}Mn_{0.4}O_{15}$. The ellipse indicates the anomaly near 570 K for $Pb_{0.8}Bi_{4.2}Ti_{3.8}Mn_{0.2}O_{15}$ and near 400 K for $Pb_{0.6}Bi_{4.4}Ti_{3.6}Mn_{0.4}O_{15}$.

rearrangements of the *A*-site cations.[18] Unfortunately, the large uncertainties in $\omega_{42}(T)$ for $x = 0.2$ and 0.4 hinder us to draw any conclusions about possible participation of the phonon mode near 42 cm^{-1} in this structural transformation in the Mn-doped compounds.

Figure 5 shows the temperature dependence of the wavenumber of the phonon mode near 220 cm^{-1}, which was attributed to TiO_6 bending and tilting in perovskite-type layers. Therefore, the anomaly in the trend $\omega_{220}(T)$ near 560 K and 400 K for $x = 0.2$ and 0.4, respectively, can be attributed to subtle changes in the octahedral layer. Anomalies at the same temperatures are seen in the corresponding $\omega_{42}(T)$ trends for both compounds, indicating the interplay between Pb^{2+} rearrangements and modifications in the octahedral tilting, as suggested by Kennedy *et al.* (2008). Similar relations have been found in the perovskite-type compounds $PbZrO_3$ and $PbHfO_3$.[54,55] This fact also shows that the amount of *A*-site Pb affects the octahedral structure. On the other hand, previous work by Zulhadjri, *et al.* on the same compounds,[8] revealed no anomaly

Table 3. The χ value in $Pb_{1-x}Bi_{4+x}Ti_{4-x}Mn_xO_{15}$ ($x = 0$, 0.2 and 0.4)

Compound	Peak position of vibration mode (cm^{-1})	χ (cm^{-1}K^{-1})
$x = 0$	270	0.0122 ± 0.0001
	870	0.0141 ± 0.0002
$x = 0.2$	270	0.0148 ± 0.0008
	870	0.0150 ± 0.0005
$x = 0.4$	270	0.0170 ± 0.0009
	870	0.0205 ± 0.0017

in the temperature dependence of the dielectric permittivity at around 570 K for $Pb_{0.8}Bi_{4.2}Ti_{3.8}Mn_{0.2}O_{15}$ and 400 K for $Pb_{0.6}Bi_{4.4}Ti_{3.6}Mn_{0.4}O_{15}$, respectively. This indicates that the incorporation of Mn in the structure smears out the structural polarity that can be detected macroscopically. The trend in temperature of $\omega_{220}(T)$ for $x = 0.4$ suggests that another structural rearrangements of the system of BO_6 octahedra might occur near 550–600 K.

The temperature dependence of the wavenumber of the phonon mode near 270 and 870 cm^{-1} showed no anomaly at the range 850–120 K and peak position of phonon mode shifted linearly to lower wavenumber. We fitted $\omega_{270}(T)$ and $\omega_{870}(T)$ using a linear function $\omega(T) = \omega_o + \chi T$ for $Pb_{1-x}Bi_{4+x}Ti_{4-x}Mn_xO_{15}$ ($x = 0$, 0.2 and 0.4). The value of the slope χ ($d\omega/dT$) can be considered as a local thermal expansion of corresponding vibrating unit. Thus, we assumed that $d\omega/dT$ for the phonon mode near 270 cm^{-1}, related to the off-centering of the *B*-site cations, is indicative of the expansibility of the polar BO_6 octahedra regarding changes in the bond angles. Whereas $d\omega/dT$ for the phonon mode near 870 cm^{-1}, which is sharpest and positioned at the highest wavenumber, represents the expansibility of the shortest *B*—O bond. The $d\omega/dT$ results are given in Table 3. It is seen that the Mn doping enhances the local octahedral deformation related to bond angles and bond lengths. Neutron diffraction studies on the same sample by Zulhadjri *et al.*[8] indicated that the introduction of Mn^{3+} on the *B*-site influences the *B*/Ti—O bond lengths, although no clear trend was established.

Conclusion

The Raman scattering of $Pb_{1-x}Bi_{4+x}Ti_{4-x}Mn_xO_{15}$ ($x = 0.2$ and 0.4) in the range 850–120 K reveals the same structural transformations as those observed in $PbBi_4Ti_4O_{15}$. The *A*-site cation displacement mode near 42 cm^{-1} as well as the octahedral tilting/bending near 220 cm^{-1} indicates a structural transformation T_a at 570 K for $Pb_{0.8}Bi_{4.2}Ti_{3.8}Mn_{0.2}O_{15}$ and 400 K for $Pb_{0.8}Bi_{4.2}Ti_{3.8}Mn_{0.2}O_{15}$. The RL mode near 60 cm^{-1} showed the structural transformation at 400 K for both compounds and at the corresponding FE–PE transition temperature 800 K for $Pb_{0.8}Bi_{4.2}Ti_{3.8}Mn_{0.2}O_{15}$ and between 750 K and 780 K for $Pb_{0.8}Bi_{4.2}Ti_{3.8}Mn_{0.2}O_{15}$.

Acknowledgements

This work was financially supported by the Desentralisasi Research Project 2012, Ministry of Education and Culture, Republic of Indonesia, IMHERE B.2c ITB 2012, Program Sandwich Luar Negeri (Prosale) 2014 and Program Publikasi Penelitian dan Disertasi 2015, Ministry of Religious Affair, Republic of Indonesia. AAN acknowledges research grant from Ministry of Research and Higher Education through Riset Kerjasama Luar Negeri dan Publikasi Internasional.

References

[1] R. S. Singh, T. Bhimasankaram, G. S. Kumar, S. V. Suryanarayana, *Solid State Commun.* **1994**, *91*, 567.
[2] A. Srinivas, M. M. Kumar, S. V. Suryanarayana, T. Bhimasankaram, *Mater. Res. Bull.* **1999**, *34*, 989.
[3] A. Srinivas, S. V. Suryanarayana, G. S. Kumar, M. M. Kumar, *J. Phys. Condens. Matter* **1999**, *11*, 3335.
[4] A. Srinivas, D. W. Kim, K. S. Hong, S. V. Suryanarayana, *Mater. Res. Bull.* **2004**, *39*, 55.
[5] N. Sharma, C. D. Ling, G. E. Wrighter, P. Y. Chen, B. J. Kennedy, P. L. Lee, *J. Solid State Chem.* **2007**, *180*, 370.
[6] N. Sharma, B. J. Kennedy, M. M. Elcombe, Y. Liu, C. D. Ling, *J. Phys. Condens. Matter* **2008**, *20*, 025215.
[7] E. V. Ramana, T. B. Sankaram, *Mater. Chem. Phys.* **2010**, *120*, 231.
[8] Zulhadjri, B. Prijamboedi, A. A. Nugroho, N. Mufti, A. Fajar, T. T. M. Palstra, Ismunandar, *J. Solid State Chem.* **2011**, *184*, 1318.
[9] S. Sun, Y. Ling, R. Peng, M. Liu, X. Mao, X. Chen, R. J. Knize, Y. Lu, *RSC Adv.* **2013**, *3*, 18567.
[10] N. A. Spaldin, M. Fiebig, *Science* **2005**, *309*, 391.
[11] W. Eerenstein, N. D. Mathur, J. F. Scott, *Nature* **2006**, *442*, 05023.
[12] N. A. Hill, *J. Phys. Chem. B* **2000**, *104*, 6694.
[13] B. Aurivillius, *Arkiv Kemi Band* **1949**, *54*, 463.
[14] B. Aurivillius, *Arkiv Kemi Band* **1949**, *58*, 499.
[15] G. A. Smolenskii, V. A. Isupov, A. I. Agranovskaya, *Fiv. Tverd. Tela (Leningrad)* **1959**, *1*, 169.
[16] R. L. Withers, J. G. Thomson, A. D. Rae, *J. Solid State Chem.* **1991**, *94*, 404.
[17] M. G. Stachiotti, C. O. Rodriguez, C. Ambrosch-Draxl, N. E. Christensen, *Phys. Rev. B.* **2000**, *61*, 14–434.
[18] A. Prasetyo, B. Mihailova, V. Suendo, A. A. Nugroho, Ismunandar, *J. Appl. Phys.* **2015**, *117*, 064102.
[19] W. Bai, C. Chen, K. Tang, J. Yang, X. Tang, J. Chu, *Ferroelectrics* **2016**, *492*, 109.
[20] B. Yuan, J. Yang, D. P. Song, X. Z. Zuo, X. W. Tang, X. B. Zhu, J. M. Dai, W. H. Song, Y. P. Sun, *J. Appl. Phys.* **2015**, *117*, 023907.
[21] K. Tang, W. Bai, J. Liu, J. Yang, Y. Zhang, C.-G. Duan, X. Tang, J. Chu, *Ceram. Int.* **2015**, *41*, S185.
[22] X. Zuo, J. Yang, B. Yuan, D. Song, X. Tang, K. Zhang, X. Zhu, W. Song, J. Dai, Y. Sun, *RSC Adv.* **2014**, *4*, 46704.
[23] G. Wang, S. Sun, Y. Huang, J. Wang, R. Peng, Z. Fu, Y. Lu, *Chin. Sci. Bull.* **2014**, *59*, 5199.
[24] E. Husson, *Key. Eng. Mater* **1998**, *155–156*, 1.
[25] P. S. Dobal, R. S. Katiyar, *J. Raman Spectrosc.* **2002**, *33*, 405.
[26] P. Colomban, A. Slodczyk, *Opt. Mater.* **2009**, *31*, 1759.
[27] J. Touluse, *Ferroelectric* **2008**, *369*, 203.
[28] B. Mihailova, B. Maier, C. Paulmann, T. Malcherek, J. Ihringer, M. Gospodinov, R. Stosch, B. Guttler, U. Bismayer, *Phys. Rev. B* **2008**, *77*, 174106.
[29] K. Datta, A. Richter, M. Gobbels, R. B. Neder, B. Mihailova, *Phys. Rev. B* **2014**, *90*, 064112.
[30] G. Gouadec, P. Colomban, *Prog. Cryst. Growth. Ch.* **2007**, *53*, 1.
[31] E. Kroumova, M. I. Aroyo, J. M. Perez-Mato, A. Kirov, C. Capillas, S. Ivantchev, H. Wondratschek, *Phase Transit.* **2003**, *76*, 155.
[32] G. De La Flor, M. Wehber, A. Rohrbeck, M. I. Aroyo, U. Bismayer, B. Mihailova, *Phys. Rev. B* **2014**, *90*, 064107.
[33] J. Liu, G. Zou, Y. Jin, *J. Phys. Chem. Solids.* **1996**, *57*, 1653.
[34] G. Zou, J. Liu, Q. Cui, H. Yang, *Phys. Lett. A.* **1994**, *189*, 257.
[35] S. Kojima, I. Saitoh, *Physica B* **1999**, *263–264*, 653.
[36] J. Liu, G. Zou, H. Yang, Q. Cui, *Solid State Commun.* **1994**, *90*, 365.
[37] S. Kojima, R. Imaizumi, S. Hamazaki, M. Takashige, *Jpn. J. Appl. Phys.* **1994**, *33*, 5559.
[38] S. Kojima, R. Imaizumi, S. Hamazaki, M. Takashige, *J. Mol. Struct.* **1995**, *348*, 37.
[39] M. Maczka, P. T. C. Freire, C. Luz-Lima, W. Paraguassu, J. Hanuza, J. Mendez Filho, *J. Phys. Condens. Matter* **2010**, *22*, 015901.
[40] M. Maczka, W. Paraguassu, P. T. C. Freire, A. G. Souza Filho, J. Mendez Filho, J. Hanuza, *Phys. Rev. B.* **2010**, *81*, 2010–104301.
[41] M. Maczka, L. Macalik, S. Kojima, *J. Phys. Condens. Matter* **2011**, *23*, 405902.
[42] K. Liang, Y. Qi, C. Lu, *J. Raman Spectrosc.* **2009**, *40*, 2088.
[43] A. Kania, A. Niewiadomski, G. E. Kugel, *Phase Trans.* **2013**, *86*, 290.
[44] J. Wang, G. X. Cheng, S. T. Zhang, H. W. Cheng, Y. F. Chen, *Physica B* **2004**, *344*, 368.
[45] H. Hao, H. X. Liu, M. H. Cao, X. M. Min, S. X. Ouyang, *Appl. Phys. A.* **2006**, *85*, 69.
[46] P. R. Graves, G. Hua, S. Myhra, J. G. Thompson, *J. Solid State Chem.* **1995**, *114*, 112.
[47] A. R. Paschoal, E. N. Silva, A. P. Ayala, I. Guedes, R. E. Alonso, A. Lopez-Garcia, A. Castro, *Ferroelectrics* **2006**, *337*, 207.
[48] R. E. Alonso, A. P. Ayala, A. Castro, J. J. Lima Silva, A. Lopez-Garcia, A. R. Paschoal, *J. Phys. Condens. Matter* **2004**, *16*, 4139.
[49] S. Kojima, *J. Phys. Condens. Matter* **1998**, *10*, L327.
[50] B. J. Kennedy, Q. Zhou, Ismunandar, Y. Kubota, K. Kato, *J. Solid State Chem.* **2008**, *181*, 1377.
[51] A. Onodera, K. Yoshio, C. C. Myint, S. Kojima, H. Yamashita, T. Takama, *Jpn. J. Appl. Phys.* **1999**, *38*, 5683.
[52] A. Onodera, T. Kubo, K. Yoshio, H. Yamashita, *Jpn. J. Appl. Phys.* **2000**, *39*, 5711.
[53] M. T. Dove, *Am. Mineral.* **1997**, *82*, 213.
[54] D. L. Corker, A. M. Glazer, W. Kaminsky, R. W. Whatmore, J. Dec, K. Roleder, *Acta Crystallogr. Sect. B: Struct. Sci* **1998**, *B54*, 18.
[55] D. L. Corker, A. M. Glazer, J. Dec, K. Roleder, R. W. Whatmore, *Acta Crystallogr. Sect. B: Struct. Sci* **1997**, *B53*, 135.